NJC

Accepted Manuscript

This article can be cited before page numbers have been issued, to do this please use: J. E. Parente, L. Naso, K. Jori, C. Franca, A. M. Da Costa Ferreira, P. A. M. Williams and E. Ferrer, *New J. Chem.*, 2019, DOI: 10.1039/C9NJ01638D.

ROYAL SOCIETY OF CHEMISTRY

rsc.li/njc

In vitro experiments and infrared spectroscopy analysis of acid and alkaline phosphatases inhibition by vanadium complexes

Juliana E. Parente[a], Luciana G. Naso[a], Khalil Jori[a], Carlos A. Franca[a], Ana Maria da Costa Ferreira[b], Patricia A.M. Williams[a], Evelina G. Ferrer[a,*]

[a]Center of Inorganic Chemistry (CEQUINOR, CONICET-CICPBA-UNLP)-Department of Chemistry-Faculty of Exact Sciences, National University of La Plata, Boulevard 120 e/ 60 y 64 (B1900AVV), 1900 La Plata, Argentina.

[b]Department of Fundamental Chemistry, University of São Paulo, Av. Prof. Lineu Prestes, 748, 05508-000 São Paulo, SP, Brazil.

To whom correspondence should be addressed (e-mail: evelina@quimica.unlp.edu.ar, Phone: 54 0221 4259485, Fax: 54 0221 445-4393). ORCID: 0000-0002-6343-5170.

View Article Online
DOI: 10.1039/C9NJ01638D

Abstract

In the course of our research of vanadium-containing complexes, two oxidovanadium complexes containing vanadium(V) and (IV) core with 4-aminobenzoic acid and/or peroxo anion as ligands were synthesized and characterized by elemental analysis, conductivity measurements, thermogravimetric analysis, and ^{1}H NMR, EPR, FTIR, UV/Vis spectroscopies. Their compositions and geometrical structures (($[VO(O_2)(C_7H_6NO_2)(H_2O)]\cdot H_2O$, $[VO(C_7H_6NO_2)_2H_2O]$) were supported by experimental data and theoretical studies (Density functional theory, DFT). The complexes were evaluated *in vitro* as phosphatase inhibitors (alkaline and acid enzymes) being considered as potential pharmaceutical agents under over-expression of those biochemical markers. The effect achieved was then analysed through FTIR spectroscopy. Changes in the finger print substrate bands as well as induced conformational changes on phosphatases enzymes secondary structure were further examined. Eventually albumin interactions experiments were performed in order to derive their bioavailability.

Keywords: vanadium complexes, phosphatase inhibition, FTIR spectroscopy, secondary structure.

View Article Online
DOI: 10.1039/C9NJ01638D

1. Introduction

Over recent years, several developments in the field of medicinal bioinorganic chemistry have taken place leading to transformations in parent drugs distribution through structural modifications of the pharmacological ligands by means of preparation of corresponding metal-based drugs. Transition metal complexes in particular present considerably more advantages compared to organic-based drugs due to the variability seen regarding coordination numbers, geometries, redox states, ligand substitution and structural diversity. Coordination to a metal ion usually leads to charge addition, and specific conformations that often ameliorate the biological activity of organic-based drugs. This novel strategy for therapy or diagnosis has come to the forefront. [1,2] There are many examples in which a synergistic effect is observed resulting in improved biological activity. Vanadium is included in this large list of metals with physiological roles; and it can be in its higher oxidation states V (V, d^0) and V (IV, d^1) in biological systems forming anionic or cationic complexes at physiological pH. Those oxidation states easily convert to each other playing an important role in the balance of reactive oxygen species which determine their intra or extra-cellular composition. In solution, vanadium exhibits rich chemistry along with its redox behaviour including the ability to form complexes with a great variety of biological molecules (ATP, ribose, glutathione, amino acids, etc). Vanadium chemical affinity to oxygen, nitrogen or sulphur atoms, as well as its flexibility in coordination geometry (tetrahedral, octahedral, to trigonal pentagonal-bipyramid for V(V), and also square pyramidal for V(IV)) allows it to form stable or transition state complexes to participate in biological process. [3,4] It was not until the 1960s that vanadium chemistry and biochemistry attracted interest with two major aspects being considered: first, biological systems and vanadium-based compounds have pharmaceutical and industrial applications; second,

View Article Online
DOI: 10.1039/C9NJ01638D

vanadium coordination complexes have further been recognized as efficient catalysts in several oxidation processes of industrial interest[5] including vanadium(V) oxo and peroxo complexes containing ligands similar to 4-aminobenzoic acid.[6] Vanadium compounds have been studied in relation to their pharmacological activities including antihyperlipidemic, anti-obesity, diuretic, antihypertensive and anticancer drugs, among others.[3,4] It was the vanadium antidiabetic effect in particular which has been attributed to the structural similarity between phosphate and vanadate anions. As a consequence, several vanadium species and organic derived compounds were successfully proven as antidiabetic agents. Their actions may include (i) enhancement of the glucose transport, (ii) inhibition of gluconeogenesis, lipolysis, and glycogenolysis in the liver and (iii) inhibition of protein tyrosine phosphatase (PTPase) and alkaline phosphatase (ALP). In this sense, vanadium dipicolinate complexes were proven to behave as insulin-mimetic compounds.[7,8]

Phosphatases display a number of physiological functions and their selective inhibitors have potential therapeutic roles. PTP1B (Protein tyrosine phosphatases 1B) belongs to a family of enzymes that catalyse the dephosphorylation of tyrosine (Tyr)-phosphorylated proteins. This phosphatase is involved in the deregulation of insulin and leptin signals which show significant for diabetes and obesity. These are part of the reasons why PTP1B becomes a therapeutic target encouraging selective inhibitors research.[9] There are many examples including alkaline (ALP) and acid (AcP) phosphatases. While the over-expression of non-specific alkaline phosphatase tissue is associated with hypophosphatasia, hydroxyapatite deposition disorder, vascular and arterial calcification, and hyperthyroidism condition[10], the elevated levels in serum of acid phosphatase are on the contrary correlated with osteoporosis and metabolic bone malignancies as well as cancer with bone metastases. AcP has indeed been identified as a relevant drug target for the treatment of bone-associated diseases.[11]

View Article Online
DOI: 10.1039/C9NJ01638D

Vanadium species are recognized as phosphatase inhibitors. Orthovanadate (VO_4^{3-}) behaves as a strong inhibitor of Na+, K+-ATPase, PTPase and ALP and also of potato and wheat germ acid phosphatases.[12] Despite the great effect showed by vanadium species, reported side effects prompted researchers to prove others vanadium organic derivative compounds as inhibitors. In effect it can be seen in the literature [3,12] that several vanadium compounds have been tested as phosphatase inhibitors. They mainly included oxidovanadium(V) and (IV) cations and bisperoxidovanadium complexes; reports pertaining to peroxidovanadium complexes, specifically those concerning AcP are, however, scarce.

All these observations encourage us to prepare, characterize and test *in vitro* the behaviour of two vanadium complexes with 4-aminobenzoic acid as ligand, based in the sequential interest of our research group in the development and study of new phosphatase inhibitors with promising bioactivities.

Finally, studies on protein carrier using fluorescence albumin experiments were performed in order to assess if the complexes can interact and be delivered by albumin at physiological conditions.

2. Materials and methods

Vanadium(V) oxide (Anedra), solid oxidovanadium(IV) sulfate pentahydrate (Merck) and 4-aminobenzoic acid (Acros Organics) were used as supplied. Peroxido species was prepared according to Fantus *et al.*[13]Bovine Serum Albumin BSA (A-6003, essentially fatty acid-free), bovine intestinal ALP (EC 3.13.1, calf intestinal mucose) and acid phosphatase AcP (EC 3.1.3.2, potato source) were obtained from Sigma Chemical

Company (St. Louis, MO) and used as supplied. All the chemicals used were from analytical grade. Elemental analysis for carbon, nitrogen and hydrogen was performed using a Carlo Erba EA1108 analyzer. Vanadium content was determined by the tungstophosphovanadic method. A Shimadzu system (model TG-50 and DTA-50), working in an oxygen flow of 50 mL.min^{-1} and at a heating rate of 10 °C.min^{-1} has been used for the thermogravimetric analysis. Sample quantities ranged between 10 and 20 mg. Al_2O_3 was used as a DTA standard.

FTIR spectra of powdered samples as pressed KBr pellets were measured with a Bruker IFS 66 FTIR-spectrophotometer in the 4000-400 cm^{-1} wavenumber range. Spectra were recorded with a wavenumber resolution of 4 cm^{-1} and 64 scans were averaged for each spectrum. The data were analyzed using OPUS program (Bruker Optics, USA).

EPR spectra in solid state were registered in an EMX Bruker instrument, working at X-band, at low temperature (77K) or at room temperature (298K). DPPH was used as calibrant. Usual instrument parameters: Power = 20.17 mW; frequency 9.42 GHz; modulation frequency 100 MHz; modulation amplitude 15G; time constant 20.48 ms.

UV/Vis spectra were recorded with a Shimadzu 2600/2700 spectrophotometer. This instrument was also used to collect the diffuse reflectance spectra, employing MgO as a standard for those experiments. Fluorescence spectra were obtained using a Shimadzu (RF6000) luminescence spectrometer equipped with a pulsed xenon lamp.

2.1. Syntheses of complexes

$[VO(O_2)L(H_2O)].H_2O$ (L= $C_7H_6NO_2$)

View Article Online
DOI: 10.1039/C9NJ01638D

Vanadium(V) oxide (0.099 g; 0.54 mmol) was dissolved in 10 ml of hot water by adding KOH 1M with heating and stirring until complete dissolution. The resulting clear yellow solution was stirred at 0ºC and the pH was adjusted at 4 (with drops of HCl 1M). To this solution, 0.15 g (1.1 mmol) of 4-aminobenzoic acid dissolved in 25 ml of distilled water was added followed by the addition of 3 mL of 10% H_2O_2 to give a red solution. The solution was left stirring (24h) and its volume was reduced by evaporation of the solvent at 60ºC to ca. 70%. The precipitated brownish orange powder was filtered out and allowed to dry at room temperature. Elemental analysis: Calc.: 31.46% C, 5.24% N, 3.74% H, 19.10% V; Exp.: 31.08% C, 4.98% N, 3.66% H, 18.81% V. TG curve: loss of one water molecule up to 160 ºC ($\Delta\omega_{exp}$ = 5.98 % and $\Delta\omega_{calc}$ = 6.74 %, DTA, endo 50 ºC). This temperature is indicative that the water molecule is not bonded to the metal, being hydration water. The complex is soluble in DMSO and DMF, partially in other organic solvents and insoluble in H_2O. For the biological measurements the complex was initially dissolved in DMSO and, thereafter a solution of the complex in a mixture of DMSO:water (5% in DMSO) was used. The values of the molar conductivities were: Ω=16.2 $S.cm^2.mol^{-1}$ (7.14 x 10^{-4} M, methanol) and Ω=21.69 $S.cm^2.mol^{-1}$ (5.53 x 10^{-4} M, DMF). It can be considered that the compound do not dissociate in solution, since for a 1:1 electrolyte, the Ω values should be ≥70 $S.cm^2.mol^{-1}$ in those solvents.[14] ^{1}H NMR spectra: Exp (Calc): H aromatic: H2a=7.72 (7.73) ppm, H3a=6.62(6.25) ppm, H5a= 6.65(6.31) ppm, H6a=7.75(7.55) ppm.[15]

[VOL_2H_2O] (L= $C_7H_6NO_2$)

To obtain this complex, 0.253 g (1 mmol) of $VOSO_4 \cdot 5H_2O$ were dissolved in 5mL of distilled water. It was then dropwise added to a solution of 0.274 g (2 mmol) of 4-

aminobenzoic acid dissolved in 45 mL of distilled water. To this solution, an aqueous NaOH 1M solution was added, under continuous stirring to a final pH value of 5. The resulting dark green solution was kept under stirring for 4 h. After that, a green precipitate was formed which was separated by centrifugation, washed several times and dried in an oven (60 ºC). Elemental analysis: Calc.: 47.06 %C, 7.84 %N, 3.92 %H, 14.28 %V; Exp: 47.52 %C, 8.20 %N, 3.70 %H, 14.25 %V. TG curve: one water molecule is lost at 180 ºC ($\Delta\omega_{exp}$ = 4.87 % and $\Delta\omega_{calc}$ = 5.04 %, DTA, endo). In this case the high dehydration temperature value indicated that the water molecule is coordinated to the metal ion. The values of the molar conductivities were: Ω=18.9 S.cm^2.mol^{-1} (7.14 x 10^{-4} M, methanol) and Ω=33.55 S.cm^2.mol^{-1} (4.47 x 10^{-4} M, DMF). It can be considered that the compound do not dissociate in solution, since for a 1:1 electrolyte, the Ω values should be ≥70 S.cm^2.mol^{-1} in those solvents.[14] ^{1}H NMR spectra: Exp (Calc): H aromatic: H2a=7.72 (7.44) ppm, H2a´=7.72 (7.58) ppm, H3a=6.62(6.23) ppm, H3a´=6.62(6.19) ppm, H5a= 6.65(6.25) ppm, H5a´= 6.65(6.30) ppm, H6a=7.75(7.60) ppm , H6a´=7.75(7.67) ppm.[15]

2.2. Phosphatases Inhibition. *In vitro* assays.

Acid phosphatase

Acid phosphatase inhibition test was performed according to Blum and Schwedt procedures.[16] The compounds solutions were prepared by diluting the stock solutions prepared in DMSO with acetate buffer (pH=5.6) to give final concentrations of 10 to 500 μM. A volume of 0.50 mL of complex solution (10-500 μM) was mixed with 0.10 mL of the enzyme solution and 1.00 mL of buffer. The mixture was kept at 37°C for 20 min (incubation time). After starting the reaction by adding 0.10 mL of the substrate solution

(*p*-nitrophenylphosphate (*p*-NPP)), the tube was kept at 37°C for more 20 min. The reaction was stopped with the addition of 0.50 mL of a 0.5 M sodium hydroxide solution. The enzymatic activity was finally calculated by measuring the absorbance of *p*-nitrophenol at 405 nm against a blank prepared without the enzyme. Three independent replicates of each point were measured. The 100% of the enzyme activity is assigned to a basal measurement containing all the reaction media including the same volume of DMSO in all the experiments. It is worthy to mention that the presence of DMSO (0.5%) did not affect the enzyme activity.

Alkaline phosphatase

The basis of the method is similar to that of AcP but differs in the pH value of the reaction medium. Again, the conversion of the substrate *p*-NPP to *p*-nitrophenol was monitored by the absorbance changes at 405 nm. Briefly, the experimental conditions for ALP specific activity measurement were as follows: 1 μg/mL of bovine intestinal ALP and 5 mM of *p*-NPP were dissolved in the incubation buffer (55 mM glycine +0.55 mM $MgCl_2$, pH=10.5) and held for 10 min. The effects of the compounds were determined by addition of different concentrations (10-500 μM) of each one to the pre-incubated mixture. The solutions of the complexes were prepared in DMSO before adding the buffer to obtain the desired final concentrations. The effect of each concentration was tested at least in triplicate in three different experiments.

2.3 Infrared spectroscopy: analysis of the substrate (*p*-nitrophenylphosphate) vibrational bands and the secondary structure of the phosphatases at the inhibition experimental conditions.

For the substrate analysis, FTIR spectra of the freeze-dried powdered samples were collected. The samples were prepared at the same experimental conditions than the *in vitro* experiments. Then, to investigate the ability of the compounds to produce conformational changes in the phosphatases enzymes, solution spectra were measured under the same experimental conditions of inhibitory experiments but without the addition of p-NPP. FT-IR/ATR spectra were recorded with a Bruker IFS 66 FTIR-spectrophotometer from 4000 to 400 cm^{-1} equipped with an internal reflectance accessory using ZnSe crystal designed to have one angle of light incidence of 45º. Spectra were recorded at room temperature with a spectral resolution of 4 cm^{-1}. To improve the signal-to-noise ratio, 200 scans were averaged for each spectrum and the procedure was performed as reported previously.[17] According to the results obtained in the previous section, the FTIR/ATR spectra of the buffer solutions (acetate buffer and glycine for AcP and ALP, respectively), AcP and ALP (at the same concentrations as the inhibition tests) and the systems: (i) ALP with 4-aminobenzoic acid (500 μM), $V(IV)O^{2+}$ (250 μM), oxidovanadium(IV) (500 μM) and peroxidovanadium(V) compounds (500 μM), (ii) AcP with 4-aminobenzoic acid (500 μM), $V(IV)O^{2+}$ (250 μM), oxidovanadium(IV) (250 μM) and peroxidovanadium(V) (500 μM) compounds were taken independently, and analyzed. Then, the absorbance values of the buffer solution were subtracted from the values of the protein solution to get the FT-IR spectra of the protein. All spectra were vector normalized in the whole range (4000-500 cm^{-1}) and were obtained after collecting and averaging 200 scans. All analyses were performed in three independent experiments, and the results were reported as averages of these replicates. The

View Article Online
DOI: 10.1039/C9NJ01638D

determination of the secondary structure was carried out on the basis of the procedure previously described.[17] The Amide I region (1700-1600 cm^{-1}) was used to investigate the secondary structure of the phosphatases in a quantitative manner. The frequencies, the number of peaks to be fitted, and the half-width of each peak to start a least square iterative curve-fitting procedures were those obtained from the second derivative of the original spectra. The areas of the bands were calculated by integration of the corresponding fitted band. A straight baseline passing through the ordinates at 1700 cm^{-1} and 1600 cm^{-1} was adjusted as an additional parameter to obtain the best fit. The curve-fitting procedure was performed by stepwise iterative adjustment towards a minimum root mean-square error of the different parameters determining the shape and position of the absorption peaks. It was carried out by assuming an initial mixed Lorentzian-Gaussian line-shape function, with full width band at half height (FWHH) of 10-15 cm^{-1} and a maximum resolution factor. Baseline corrections, normalization, derivation, curve fitting and area calculation were carried out by means of Grams/32 (Galactic Industries Corporation, USA) software, OPUS 3.1, and Perkin-Elmer software. The resulting fitted curve was analyzed taking into account the following assignments: β-sheets, 1637-1613 cm^{-1}; solvated helix, 1625-1637 cm^{-1}, random coil, 1645-1637 cm^{-1}, α-helix, 1658-1650 cm^{-1}, turns, 1673-1666 cm^{-1} and β-antiparallel, 1695-1675 cm^{-1}. In order to calculate the percentage contribution of the different types of conformations to the area of all the components, bands assigned to a given conformation were summed and divided by the total Amide I area.

2.4. Albumin interaction

Fluorescence quenching experiments

Bovine serum albumin (BSA) was dissolved in 0.1M Tris-HCl buffer (pH 7.4) to attain a final concentration of 6 μM. The solutions of the studied compounds were added drop-wise to the above 6 μM BSA preparation to ensure the formation of a homogeneous solution and to obtain the desired concentration of 0-100 μM. Adequate solubility was reached under these experimental conditions and the compounds did not showed significant fluorescence that could interfere with the measurements. For each sample and concentration, three independent replicates were performed at 25 ºC and 37 ºC. BSA 6 μM was titrated by successive additions of complex solutions from 0 to 100 μM and the fluorescence intensity was measured (excitation at 280 nm and emission at 348 nm). All the fluorescence quenching data were analyzed according to previous studies performed in the laboratory by applying a traditional mathematical procedure. The fluorescence-quenching mechanism has been analyzed using the Stern-Volmer eq. (1).[18]

$$F^o/F = 1 + K_{sv}[Q] \qquad \textbf{eq. (1)}$$

where F^o is the steady-state fluorescence intensity of BSA alone while F is the observed intensity upon increasing the quencher concentration, K_{sv} is the Stern-Volmer quenching constant and [Q] is the quencher concentration. Usually, the curve of F^o/F vs [Q] is linear if the type of quenching involves a unique process: static or dynamic. Static quenching is due to the complex formation between the fluorophore and the quencher. It can be distinguished from collision effects because generally the K_{sv} value is higher than the value of the dynamic quenching constant (K_q). Considering that $K_q = K_{sv}/\tau_0$ (where $\tau_0 = 10^{-8}$ s is the average lifetime of the biomolecule without quencher), this constant can be estimated and compared with the maximum diffusion collision quenching rate constant (reference value from the literature) which is 2×10^{-10} M^{-1} s^{-1}. If the K_{sv} value is greater, then a mechanism of interaction through the complex formation can be proposed. Otherwise it would be a collisional quenching. If the quenching is static, it is assumed that there are

View Article Online
DOI: 10.1039/C9NJ01638D

specific binding sites. These binding sites, and their association constants, were estimated using the following mathematical relationship:

$$\log [(F^0-F)/F)] = \log K_b + n \log [Q] \quad \textbf{eq. (2)}$$

where K_b is the binding constant and *n* is the average number of biding site per protein molecule.

To obtain information about the type of interaction, the thermodynamic parameters were calculated using Van´t Hoff equation[18]:

$$\ln (K_{b2}/K_{b1}) = -\Delta H^0/R\ (1/T_2-1/T_1) \quad \textbf{eq. (3)}$$

where T_1 and T_2 are the absolute temperatures at which K_{b1} and K_{b2} were determined. The standard free energy change (ΔG^0) and the standard free entropy change (ΔS^0) were evaluated according to the well-known thermodynamic relationships:

$$\Delta G^0 = -\ RT \ln K_b \quad \textbf{eq. (4)}$$

$$\Delta S^0 = (\Delta H^0-\Delta G^0)/T \quad \textbf{eq. (5)}$$

3D fluorescence spectra

The three-dimensional fluorescence spectra were performed under the following experimental conditions: (i) Emission wavelength was recorded between 200 and 600 nm, (ii) Excitation wavelength from 200-400 (5 nm of increment), (iii) the number of scanning curves was 15. Other scanning parameters were just the same to those of the fluorescence quenching spectra.

View Article Online
DOI: 10.1039/C9NJ01638D

2.5. Computational methods

The absence of X-ray single-crystal analysis led us to characterize the structures of the complexes using Gaussian 09 program[19] and the density functional theory (DFT) calculations which have demonstrated a good correlation with experimental data for coordination metal complexes. Truhlar model M06L[20] was used to optimize the geometries based on a meta-GGA functional. Basis sets of triple-zeta quality with polarized (TZVP) functions were used for all atoms. The initial structures of the complexes were modeled as isolated molecules according to the experimental data for the complexes and taking into account the solvent environment using the conducting polarizable continuous model (CPCM) as implemented in the software package. The ground state geometries were optimized using the method mentioned above in the gas phase. The vibrational analysis were performed at the same level of theory in order to get a minimum on the potential energy surface, and then, calculation of IR and Raman frequencies were considered for supporting the characterization of the complexes. UV-vis spectra were calculated with the time-dependent density functional theory (TD-DFT) formalism[21] using the well-known functional B3LYP[22,23] and a split-valence triple zeta basis set (6-311+g*). Solution spectra were carried out simulating solvent effect using the same model described above. Water and DMF were taken into account for optimization and UV/Vis, respectively.

3. Results and discussion

Experimental data (elemental analysis, thermogravimetric, conductimetry, ^{1}H NMR), physicochemical characterizations (see above) together with theoretical optimized structures analysis, let us to propose the following structures to the studied complexes,

View Article Online
DOI: 10.1039/C9NJ01638D

showed in Figure 1. In the peroxido complex $[VO(O_2)L(H_2O)]\cdot H_2O$, the vanadium center is located in a pentagonal pyramid with a bidentate coordination mode of the peroxo and the carboxylate group of the 4-aminobenzoate ligand. A water molecule occupied the equatorial position forming a distorted pentagonal plane (Figure 1A). For the oxidovanadium complex *cis*-$[VOL_2H_2O]$, the oxidovanadium(IV) cation shows a distorted octahedral structure being both 4-aminobenzoate ligands in a bidentate coordination mode through the carboxylate groups and a water molecule complete the six-coordination sphere. From the two calculated possible conformations (*cis*- and *trans-)* the *cis*-one was in correspondence with the experimental results (see below), showed in Figure 1B (see Figure S1 for *trans* structure). Characteristic bond lengths and angles around the vanadium atom for the complexes are depicted in Table 1.

3.1. Infrared Spectra

The FTIR spectrum was analyzed in comparison with the corresponding spectrum of 4-aminobenzoic acid which has been extensively studied.[15] The most characteristic bands are shown in Table 2. (Figure S2).

The FTIR spectra of the complexes display typical features of the coordinated ligand when they were compared with the spectra of 4-aminobenzoic acid and its sodium salt. The calculated spectra for $[VO(O_2)L(H_2O)]\cdot H_2O$ and $[VOL_2H_2O]$ were used to support empirical assignment of the vibrational bands. Table 2 shows that the experimental and the selected calculated wavenumbers for the compounds are in good agreement even without the use of scaling factors. The differences observed are related to the fact that the

calculations for the isolated molecule have been performed in gas phase and the experimental spectra correspond to solid samples.

As it is well known, the formation of an ionic salt from a carboxylic acid produces two bands related to the ionic form of the carboxylate group corresponding to the asymmetric $\nu_{as}(COO^-)$ and symmetric $\nu_s(COO^-)$ stretching modes.[24] Thus, the 1680 cm^{-1} band of the ν(C=O) stretching of the carboxylic acid group is splitted into two components at 1529 cm^{-1} and 1397 cm^{-1} in the sodium salt giving a $\Delta\nu$ ($\nu_{as}(COO^-)$-$\nu_s(COO^-)$) value of 132 cm^{-1}. Other characteristic bands are due to the presence of the -NH_2 group in the molecules of both (the free acid and the sodium salt). They appear in the ranges of 1620-1635 cm^{-1} for the $\delta(NH_2)$ and 1070-1085 cm^{-1} for the δ(HNC) vibrational modes. Analyzing the FTIR spectrum of the *cis*-oxidovanadium(IV) complex, two new bands at 1506 cm^{-1} and 1408 cm^{-1} can be clearly seen. These bands can be assigned to the asymmetric stretching ($\nu_{as}(COO^-)$) and symmetrical stretching ($\nu_s(COO^-)$) vibrational modes, respectively. The same vibrational modes appear at 1525 cm^{-1} and 1429 cm^{-1} in the peroxidovanadium(V) complex. In both cases the calculated $\Delta\nu$ values (98 and 96 cm^{-1}, respectively) are lower than the $\Delta\nu$ of the sodium salt suggesting a bidentate type of coordination of the carboxylate group to vanadium.[24] In addition, the ν(V=O) stretching bands can be detected. They appear at 965 cm^{-1} for the oxidovanadium(IV) complex. It was established that the decrease of ν(V=O) stretching frequency which occurs in oxidovanadium complexes is a measure of the donor ligand capacity. From the differences observed between the calculated and experimental ν(V=O) frequencies values of the oxidovanadium(IV) complex, the lowest value is shown by the *cis*- configuration which has a longer V=O distance (see electronic supplementary information). This is in correspondence with the presence of one water molecule in the equatorial plane of the oxidovanadium(IV) complex having less electron donation ability than the carboxylate

View Article Online
DOI: 10.1039/C9NJ01638D

group as it was expected.[25] For the peroxidovanadium(V) complex (with a shorter bond length, see Table 1) this band can be detected at higher wavenumbers (998 cm^{-1}) and has been assigned to a combined vibration of V=O and O-O bonds due to their mutual interactions. Additionally, the vibrational modes corresponding to the characteristic stretches $\nu(V\text{-}O_2)$ of the peroxo moiety can be assigned to the 668 and 630 cm^{-1} bands (associated to the deformation mode $\delta(OOV)$ in the case of the lowest wavenumber). These assignments agree well with previous studies for peroxido heteroligand vanadate complexes.[26]

The IR spectra of the complexes exhibit a broad absorption band in the 3300-3400 cm^{-1} region and the νNH_2 vibration bands cannot easily been assigned. Thus, lower frequencies of the FTIR spectra were analyzed. In relation to the presence of the NH_2 group in the molecule, it is well known that the N-H bond in both, primary and secondary amines, are polar having a partial charge density on H and a negative partial charge density on N. This gives to the group the ability to form hydrogen bonds.[27] In the Table 2 (Figure S2), the shifts of the bands assigned to vibrational modes of the NH_2 group can be observed. According to the theoretical assignments, this band is actually composed of two contributions $\delta(NH_2)$ and $\nu(CC)$ (Table 2) with varying intensity ratios. For $[VO(O_2)L(H_2O)].H_2O$ the ratio is 3:1 $\delta(NH_2)$: $\nu(CC)$ in contraposition of the 1:1 relationship for $[VOL_2H_2O]$ and probably that is the reason why they appear with different intensities in the FTIR spectra. In addition, the possibility of neighboring interactions produced by the solid phase cannot be excluded. It can be noted that this combined band shifted to higher wavenumber in comparison with the sodium salt and the ligand, suggesting that the formation of the metallic complex provoked the rupture of the hydrogen bonds causing the increment of the wavenumber values as a consequence of the shortening of the NH bonds.[28]

3.2. Diffuse reflectance and UV/Vis spectroscopy. Solution stability.

The electronic spectra of the solids compounds and the behavior of the complexes in solution were studied using diffuse reflectance and UV-vis spectroscopy in order to characterize the complexes and to compare the species formed in solid phase with the species present in solution.

Both complexes behaved as expected in solid phase and in solution. The solid peroxidovanadium(V) complex showed the typical bands associated with the CT of the amino and peroxo groups which appear at c.a. 455 nm, 385 nm and 318 nm (460 nm, 392 nm and 314 nm from the fitting and deconvolution process; Figure 2(A) ((a) and (b), respectively).[29] It is well known that UV-vis spectroscopy is a very useful tool for identification of mono- or di- peroxido complexes. The absence of the peroxido-vanadium charge transfer band (c.a. 220 nm) implies the presence of the peroxido vanadium species. Usually, peroxidovanadium(V) complexes showed one absorption band in the region 400-460 nm and other CT band assigned to a L→M (peroxo to vanadium) (c.a. 325 nm) (Figure 2A(a)). In addition, the calculations performed (considering the solution spectra) support these assignments. Based on the theoretical calculations (Figure 2 (B, b)), the observed characteristic bands in the UV-vis spectra can be assigned as follow: 400 nm (HOMO → LUMO, H-1 → LUMO), ligand charge transfer (aminobenzene and peroxo) to metal; 342 nm (H-1→ L+2), ligand charge transfer (peroxo) to metal; 293 nm (H-1→ L+2, L+5), ligand charge transfer (peroxo) to ligand (aminobenzene) (Figure S3). The two last transitions are typical for peroxidovanadium species. Solution spectrum (2.7×10^{-3} M, DMF, Figure 2B(a)) showed similar pattern band with splitting of the band around 300 nm. The most intense bands are displayed at 303 nm (ε = 525.9 $M^{-1}.cm^{-1}$), 330 nm (ε = 540.7 $M^{-1}.cm^{-1}$) and 407 nm (ε = 129.6 $M^{-1}.cm^{-1}$). Similar pattern was obtained from the fitting and

deconvolution process which is also consistent with the simulated solution spectrum (Figure 2 (A, B)).

The solid oxidovanadium(IV) complex usually shows d-d absorption bands. Three absorptions are expected: $b_2(dxy) \rightarrow e$ (dxz, dyz) (1000-670 nm), $b_2(dxy) \rightarrow b1$ (dx^2-y^2) (667-555 nm), $b_2(dxy) \rightarrow a_1$ (dz^2) (417-345 nm), being the last one usually overlapped for a charge transfer band from the ligand. In this case, the reflectance spectrum of the oxidovanadium(IV) complex showed two characteristic d-d bands, one located > 850 nm and other at 623 nm corresponding to the two lower energy transitions according to Ballhausen-Gray energy level scheme (Figure 3A).[30] Solution spectrum (0.11 M, DMF) showed bands at 400-900 nm region which can be assigned to the electronic d-d-transitions of $b_2 \rightarrow b_1$ (480 nm, ε =25.18 $M^{-1}.cm^{-1}$) and $b_2 \rightarrow e$ (864 nm, ε = 27.54 $M^{-1}.cm^{-1}$; 740 nm (shoulder, ε = 23.72 $M^{-1}.cm^{-1}$) (Figure 3B). Solvent effect, possibly caused by the replacement of the water molecule in the equatorial position, or axial coordination around the metal center, provoked a blue shift of these bands in comparison with the solid reflectance spectrum. The *cis*- conformation for the oxidovanadium(IV) complex is additionally supported by the calculated *cis*-UV/Vis spectrum. The spectrum of the *cis*-conformation exhibits a good correlation with the experimental one (Figure 3C) having a similar pattern with two bands in opposition with the simulated for the *trans*-one. The observed splitting of the UV/Vis band is usually expected as a consequence of the symmetry lowering.[31] According to the calculations, the bands were assigned to 733 nm (H-2 → L) and 548 nm (H-2 → L+4) and correlates reasonably well with the experimental spectrum (Figure S4).

Both complexes remained stable in a DMF and DMSO solutions (no appreciable changes were observed in the UV/Vis spectra, data not shown) at least during 1h. Then, it

can be stated that the complex did not decompose during the manipulation of the solutions for the *in vitro* biological assays.

3.3. EPR spectroscopy

The suggested coordination mode in the oxidovanadiun(IV) complex interpreted by FTIR (Experimental and theoretical), diffuse reflectance and UV/Vis spectroscopy, and supported by the theoretical analysis was also substantiated by EPR measurements.

The X-band EPR powder spectrum of the $[VOL_2H_2O]$ complex, recorded at room temperature, is shown in Figure 4A. The main feature is a broad and isotropic signal with a g_0 value of 1.961 which is in concordance with a nearly axial ligand field as is usually observed for vanadium complexes owing vanadium-oxygen interactions (O-V-O) in the oxidovanadium(IV) unit.[32] Some weaker signals are also observed superposed on the central line; they correspond to the hyperfine structure of a V(IV) isolated species (100% abundant ^{51}V nucleus with I = 7/2).

In order to establish the binding mode of the ligand and to identify the bioactive solution species of the $[VOL_2H_2O]$ complex, EPR studies of the dissolved powder were performed. Figure 4B, shows the signal obtained in a DMF solution, at 298 K. The EPR signal shows the typical eight-line pattern spectrum for the oxidovanadium(IV) cation systems indicating the formation of single mononuclear species after the dissolution process. The spectral simulation, by the Bruker Simfonia program, predicted the formation of an oxidovanadium(IV) chromophore with spin Hamiltonian parameters of $g_0 = 1.988$ and $A_0 = 108.3$ G (100.5×10^{-4} cm^{-1}). This signal is coincident with the formation of oxidovanadium(IV) complexes with oxygen containing ligands and solvation at the *cis*-

View Article Online
DOI: 10.1039/C9NJ01638D

position in which the isotropic hyperfine coupling constant is larger than that obtained for the *trans*- isomer.[33] The reduction of the hyperfine splitting constant value (A_0) and the increment of the g_0 parameter is expected, in comparison with those to the oxidovanadium(IV) free cation ($V(IV)O^{2+}$, $g_0 = 1.964$ and $A_0 = 106.3 \times 10^{-4}$ cm^{-1}),[34] when negatively charged carboxylate groups are in the first coordination sphere.

3.4. Biological activities

3.4.1. Acid (AcP) and alkaline (ALP) phosphatase inhibition assays

As mentioned above, researchers are excited in the development of chemotherapeutic agents.[35] Simple salts and several vanadium(IV) and (V) complexes have demonstrated inhibition abilities against phosphatases.[36] Based on this assumption, the inhibition ability of the peroxidovanadium(V) and oxidovanadium(IV) complexes were determined.

In both assays, the activity of the free ligand, oxidovanadium(IV) sulfate and peroxidovanadium(V) species was also assessed. In Figure 5A it can be observed the AcP inhibition experiments. The free ligand had no inhibitory effect on AcP. The peroxidovanadium(V) complex did not inhibit phosphatase activity and its activity remained almost constant up to the higher tested concentrations (100-500 μM). On the other hand, the oxidovanadium(IV) complex inhibits the enzymatic activity. It was less efficient than the oxidovanadium(IV) sulfate, resulting in a 50% of inhibition of the activity at a concentration of 250 μM (IC_{50}).

The data in Figure 5B showed the inhibitory effects of the compounds on the ALP at various concentrations. The ligand 4-aminobenzoic acid, the peroxidovanadium(V) species and the oxidovanadium(IV) complex showed no significant inhibition.

Surprisingly, the peroxidovanadium(V) complex exerted better inhibition than the oxidovanadium(IV) sulfate salt from concentrations higher than 50 μM reaching at a 50% of inactivation of the enzyme at 500 μM concentration value.

Amino derivative vanadium complexes demonstrated specific activity against phosphatases. The studied oxidovanadium(IV) complex behaves as a better inhibitor toward acid phosphatase, whereas peroxidovanadium(V) complex has superior inhibition effect on ALP.

It would be possible to find tentative explanations for these behaviors based on the following considerations. In a previous work, McLauchlan *et al*[36] performed a series of inhibition experiments on alkaline phosphatase (bovine calf intestine) and acid phosphatase (wheat germ) employing vanadium complexes containing the bidentate ligand picolinate and the metal in (III), (IV) and (V) oxidation states. They concluded about the relevance of the oxidation state and provided evidence that, in general, the most effective inhibitors are the complexes with an oxidation state of (V). Thus, one of the factors involved in the difference in the effect on ALP of $[VOL_2H_2O]$ and $[VO(O_2)L(H_2O)]\cdot H_2O$ complexes could possibly be associated to the oxidation state of vanadium. Indeed, it was proposed that for the alkaline phosphatase the complexes containing vanadium are more efficient in an oxidation state of (V).[37]

It might also be thought that the optimum pH values for enzymatic action could be related to these differences in their activity. It is well known that oxidovanadium(IV) species are more stable close to neutral pH range in opposition to the effect of vanadium(V) species.[38]

Electronic nature of ancillary ligands is another factor that could be taken in consideration in the physiological effects of vanadium complexes. In experiments of

View Article Online
DOI: 10.1039/C9NJ01638D

cytotoxicity on Rat hepatoma H4IIEC3 cells, a series of peroxidovanadium(V) complexes with pentagonal-bipyramidal structure have been tested.[39] It has been found that the IC_{50} values are greater than those produced by a 1:1 mixture of hydrogen peroxide and sodium orthovanadate and concluded that the incorporation of organic ligand moderates the cytotoxicity of vanadium, and that the electronic properties of the peroxo group affected the physiological activity of the complexes. Ziegler *et al.* studied the inhibition potency of a series of systematically modified oxidovanadium(IV)-β-diketone complexes.[40] They analyzed the inhibitory potency on calf-intestine alkaline phosphatase and correlated the calculated charge on VO unity with the effect of each metal complex. Their conclusion supports the idea that a more positive center led to the complex more tightly bound to the enzyme, and consequently behaving as a stronger inhibitor agent. If we assume this possibility and evaluate the calculated Mulliken charge on the VO group for $[VOL_2H_2O]$, and compare the data with that calculated for the $[VO(O_2)L(H_2O)]\cdot H_2O$ complex, these values are 0.50 and 0.64 (a.u.), respectively. Then, it can be proposed that peroxidovanadium(V) complex acts as a more positive center than oxidovanadium(IV) complex against ALP. Considering as well as the others factors, it can be assumed for neutral complexes that electron density on vanadium ion affects the enzyme interaction or the membrane transport.

In summary, the prevalence of oxidation state, the coordination number that complex adopts in solution, the pH and the electron density on VO group do possibly affect significantly their activities. We cannot discard others factors involved as the type of interaction, mechanism of inhibition, stability, etc., but further studies are needed to elucidate them.

It can also be mentioned that $VO(O_2)^+$ species was able to inhibit in a stronger manner the acid phosphatase (potato source), contrary to its effect on the acid phosphatase

from wheat germ (Figure 5A).[41] Furthermore, it is evident that peroxidovanadium(V) complex did not inhibit AcP. There is not so much information about inhibitory power of peroxidovanadium complexes, but potent inhibition on AcP has been related to the greater affinity of the inhibitors for imidazole nitrogen of the enzyme. Nevertheless, acid phosphatases from different sources may provide different inhibitions capacity for the same vanadium compound.[42]

Some aspects revealed in this work can be discussed in association with other previous reported vanadium-based phosphatase inhibitors (Table 3). To provide a comparative analysis, the presences of free NH groups as well as the influence of the phenyl group as part of the ligand were considered. Phenyl moiety was selected to explore if such types of compounds would be more portent inhibitors considering their structural relationship with phenol and the PNPP substrate. The formation of vanadate phenyl ester, produced an improvement of the inhibition ability of vanadate alone.[43,44]According to these studies, vanadate in presence of phenol significantly improved the inhibition potency on *E. coli* alkaline phosphatase due to the formation of species analogous to organic phosphate esters.[44]

The results of McLauchlan *et al* [36] demonstrated that, in the case of vanadium complexes containing the ligand imidazole-4-carboxylate (imc), the values for the Michaelis binding constant (K_m) showed that $VO(imc)_2$ complex had the lower K_m = 3.3 μM value denoting stronger affinity for wheat germen acid phosphatase and, the greater K_m values were for ALP and PTP1B in opposition to the data observed for the $VO_2(imc)_2^-$ (Table 3). This affinity is comparable in some way to the results obtained in this work where the oxidovanadium(IV) complex behaved as a better inhibitor of the AcP and the peroxidovanadium(V) complex of the ALP. The anthranilate (2-aminobenzoate) vanadium complexes ($VO(anc)_2$, $VO_2(anc)_2^-$) worked in a similar way for PTP1B but not for AcP.

View Article Online
DOI: 10.1039/C9NJ01638D

These results are possible due to the lack of the free NH groups because contrasting 4-aminobenzoate vanadium complexes they are involved in the coordination to the metal center. Structurally similar complexes with phenyl derivative ligands were $VO(trop)_2$ and $VO(hino)_2$[45] (Table 3). Both were tested on PTP1B denoting higher inhibition activity for the $VO(hino)_2$ complex. The difference between the ligands is that the hino ligand has an additional $–CH_2(CH_3)_2$ group attached to the benzoic moiety. This structural modification causes the reduction in 50 % of the IC_{50} value. $VO(imc)_2$ and $VO(hino)_2$ complexes could also be compared. Regardless the differences of the experimental method, K_m value for $VO(hino)_2$ is significantly lower (0.15 μM) than for $VO(imc)_2$ (43 μM). The hypothesis concerning to the vanadium delivery to the active site of the enzyme could be the explanation of the inhibition ability of $VO(hino)_2$. Possibly, the VO_4 coordination sphere was more favorable for vanadate formation.[4,12,36,44] Ligand selectivity is also observed when biguanide oxidovanadium(IV) complexes ($[VO(Big)_2].H_2O$, $[VO(Big1)_2].2H_2O$) were compared.[46] The oxidovanadium complex that contain the phenyl group as part of the ligand acted as a better inhibitor on ALP than on PTP1B. Another example arises from the comparison between dioxidovanadium(V) complexes $[VO_2(L^1)]_2[(Et)_3NH]_2$ (L^1= 2,4-(dihydroxyphenyl)ethylidene)benzohydrazide) and $[VO_2(L^2)]_2[(DBU-H)]_2$ (L^2 = bis[(3-hydroxy-5-(hydroxymethyl)-2-methylpyridin-4-l)methylene]oxalohydrazide).[47]The complex having L^1 ligand was an efficient PTP1B inhibitor (Table 3).

As it was stated, there is scarce information related to inhibition ability on AcP, ALP or PTPB1 of peroxidovanadium(V) complexes having a structurally related ligand to 4-aminobenzoate anion. However, the following examples can be considered. Water-soluble polymer matrices containing bis-peroxo vanadium complexes ($[VO(O_2)_2$(sulfonate)]-PSS, $[V_2O_2(O_2)_4$-(carboxylate)-$VO(O_2)_2$(sulfonate)]-PSSM) have been proved on ALP and contrasted with $Na[VO(O_2)_2(H_2O)]$ (Table 3).[48] The

bisperoxidovanadium(V) polymeric complexes were more effective than the peroxidovanadium(V) vanadium complex ([$VO(O_2)L(H_2O)$]). Interestingly, the peroxide species ([$VO(O_2)]^+$) did not inhibit intestinal ALP whereas the bisperoxide showed inhibitory activity (IC_{50}=25.18 μM). This marked difference in reactivity may be possibly associated to the aqueous stability of perovanadates.[49]

Finally, the peroxido complexes [$VO(O_2)L(H_2O)]\cdot H_2O$ (L=4-aminobenzoate) and NH_4[$VO(O_2)$(dipic)(H_2O)][50]·have acted as ALP inhibitors (Table 3). As it was shown, in [$VO(O_2)L(H_2O)]\cdot H_2O$ the vanadium center is located in a pentagonal pyramid with a bidentate coordination mode of the peroxo and the carboxylate group including a water molecule in the equatorial position. In NH_4[$VO(O_2)$(dipic)(H_2O)] complex the vanadium atom environment is a seven-coordinate distorted pentagonal bipyramid with the vanadyl oxygen and the water molecule at the apices and the peroxo group, nitrogen and two monodentate carboxylate groups in the pentagonal plane. It can be assumed that in solution the [$VO(O_2)L(H_2O)]\cdot H_2O$ complex may adopt a seven coordinate structure similar to NH_4[$VO(O_2)$(dipic)(H_2O)] thus it could be suggested that this type of structural arrangement around vanadium(V) tends to favor enzyme inhibition.

3.4.42. Analysis of the inhibitory effect by FTIR spectroscopy

(i) Substrate (*p*-nitrophenylphosphate) bands

The inhibition or the stimulation effect can be clearly seen by studying the FTIR changes in the finger print region (1230-840 cm^{-1}) of the substrate (*p*-nitrophenylphosphate) corresponding to the phosphate group vibrations upon enzymatic or non-enzymatic hydrolysis.[51]

View Article Online
DOI: 10.1039/C9NJ01638D

Lyophilized blank solution containing all the reactants, except ALP enzyme, showed the presence of the typical phosphate bands: 1115 cm^{-1}, 1043 cm^{-1} and 981 cm^{-1} [52] (Figure 6). There was a drastic lowering in the 1115 cm^{-1} band intensity (50%) as a consequence of the ALP action on the phosphate hydrolysis. When the 4-aminobenzoic acid or the oxidovanadium(IV) complex were included in the reaction media, there was no significant changes in the intensity of the main band of the substrate observed at 1115 cm^{-1} with respect to the control with ALP. There is some decrease in the intensity of the 980 cm^{-1} band that may imply some kind of interaction between the phosphate group and those compounds. Besides, no interference with the corresponding bands of ν(V=O) stretching frequencies of the oxidovanadium(IV) (965 cm^{-1}) and peroxidovanadium(V) (998 cm^{-1}) complexes has been observed, due to the low concentration of the complexes. In opposition, in the presence of the peroxidovanadium(V) complex, the spectrum showed that the intensity of the band related to the phosphate group did not significantly decrease in comparison with the spectrum of the blank, suggesting lack of the phosphate hydrolysis process in concordance with the inhibition effect.

Unfortunately in the case of the AcP, the obtained FTIR spectra did not passed the quality test in order to be analyzed.

(ii) Conformational changes in the secondary structure of phosphatase enzymes

There are some studies that use FTIR spectroscopy to analyze the conformational changes that occur on the secondary structure of the phosphatases under different type of conditions as hyperbaric manipulation[53], thermal and pH modifications[54], interaction with some metal ions[55] or with tartaric acid.[56] It was known that the main spectral features of

View Article Online
DOI: 10.1039/C9NJ01638D

both enzymes are the characteristic strong Amide I band located at c.a. ~1658 cm^{-1} which is indicative of the predominance of the α-helix conformation on the secondary structure.[55,56] It is also well established that an attachment of any compound to the enzyme is able to produce conformational changes that can be observed by FTIR spectroscopy analyzing the different components of the Amide I band. In this section, a quantitative analysis of each conformational component such as α-helix, β-sheet, turns, solvate helix and random coil structures is provided in order to get a deeper insight about the possible modifications that the inhibitors provoke on enzyme structure.

As it can be seen from Table 4, the curve-fitting procedure based on the second derivative spectra indicated that the α-helix content of the ALP control sample is about 39.59%. The interaction of oxidovanadium(IV) complex and 4-aminobenzoic acid (non-inhibitors) did not produced remarkable changes on the Amide I components. The α-helix conformation slightly decreased (~13-14%) whereas the most remarkable change is the increment in percentage of the β-antiparallel structure. The observed losses of the percentages of α-helix native structure, accompanied by the increment of the β-antiparallel structure did not affect in a great extent the main conformation of the enzyme. This is consistent with the maintenance of the structure integrity of the ALP enzyme and its activity as a consequence. On the contrary, a drastic reduction in the α-helix conformation (~40%) was observed for the compounds that produced inhibition on the ALP activity (peroxidovanadium(V) complex). This loss of the α-helix (un-solvated) conformation was cooperative with the gain of solvated α-helix structure. Those changes can be explained in terms of the solvent accessibility. The native α-helix (1650-1658 cm^{-1}) is shown to be protected from the solvent by a tertiary fold. However, in the absence of this protection the helix become solvated and a spectral band at c.a. ~1630 cm^{-1} appeared in the FTIR

View Article Online
DOI: 10.1039/C9NJ01638D

spectrum.[57,58] It is then suggested that under the presence of inhibitors, the secondary structure of ALP became more flexible and more exposed. As a result, ALP allows the compounds to interact producing structural changes that block its activity. There was no presence of random coil structure component (1637-1645 cm^{-1}) in the ALP analyzed samples.

In the case of the AcP inhibitor, the oxidovanadium(IV) complex (Table 4), a rearrangement involving a lowering in the percentage contribution of α-helix and random coil structures, and a remarkable increment in the percentage of the solvated helix structure were produced. Again, the solvent accessibility could be involved but there was an additional structural modification: a decrease of 20% in the percentage of the random coil component that could led to AcP activity inhibition.

4. Albumin interactions

Because serum albumin is one of the most abundant transporter-protein in plasma, the affinity of drugs towards albumin can be correlated with a better accessibility to the target. Albumin plays an essential role in the increment of solubility and in the cellular delivery of compounds present in blood. For that reason the study of the interaction of selected compounds with the protein have significance in the binding properties of the complexes.

Fluorescence quenching experiments were performed for the peroxidovanadium(V) complex. The intensity of the complex band was negligible with respect to the band corresponding to its interaction with albumin. A decrease in the albumin fluorescence intensity was observed when measurements were performed at fixed BSA concentration (6 μM) and increasing concentrations of the peroxidovanadium(V) complex varying from 1 to

100 μM. The fluorescence quenching data were analyzed by the Stern-Volmer equation. The plot F^0/F vs [Q] showed a positive deviation indicating the presence of both static and dynamic quenching[59] by the same fluorophore (Figure 7, left). Assuming one type of quenching process at lower concentrations, K_{sv} constant were evaluated at the two temperatures (Figure 7, left, inset) and the calculated values were $K_{sv} = 3.92 \times 10^4\ M^{-1}$ (298K) and $K_{sv} = 3.58 \times 10^4\ M^{-1}$ (310K). In addition, the quenching rate constant K_q could be estimated through the relationship $K_q = K_{sv}/\tau_0$ (τ_0 = average lifetime of the biomolecule without quencher assumed to be 10^{-8} s for the fluorescence lifetime of the biopolymer). Then, both estimated K_q values $3.92 \times 10^{12}\ M^{-1}.s^{-1}$ (298K) and $K_{sv} = 3.58 \times 10^{12}\ M^{-1}.s^{-1}$ (310K) resulted higher than the maximum scatter collision quenching constant of various quenchers with the biopolymer ($2 \times 10^{10}\ M^{-1}.s^{-1}$).[47] Consequently, static type of quenching can be assumed involving a compound formation between the complex and BSA. Furthermore, from the plot log[(F^o-F)/F] versus log[Q] (Figure 7, right), the binding constants and the number of binding sites, were calculated being $K_b = 2.29 \pm 0.01 \times 10^5\ M^{-1}$ (298K) and $K_b = 1.82 \pm 0.01 \times 10^5\ M^{-1}$ (303K), and n~1 at both temperatures. It is well acknowledged that reversible binding to one high-affinity sites of the albumin is accompanied by association constant (K_b) values from 10^4 to $10^6\ M^{-1}$ indicating a carrier-like behavior.[60] Thus, the K_b values of the complex suggested that it could be transported by BSA and that there were no significant differences in the binding ability at both temperatures. In addition, the value of n~1 suggested that there is almost one class of binding site to peroxidovanadium(V) complex at BSA. Finally, to analyze the acting forces between the complex and albumin, thermodynamic parameters were evaluated, in which ΔG^o= -30.56 KJ/mol, ΔH^o = 14.69 KJ/mol and ΔS^o= 151.84 J/K.mol. The negative value of $\Delta G°$ indicates that the interaction of the complex with BSA is spontaneous and the driving force is mainly an entropic factor. The values of both $\Delta H°$ and $\Delta S°$ are positive, which

View Article Online
DOI: 10.1039/C9NJ01638D

suggested that the main contribution to these changes arise from hydrophobic interactions.[61]

Due to the interference of 4-aminobenzoic acid and oxidovanadium(IV) complex in the fluorescence quenching experiments, their interaction with BSA was studied examining UV/Vis and 3D fluorescence spectra.

UV/Vis spectroscopy is a simple method to investigate structural changes in BSA and determine complex formation. BSA shows a characteristic UV/Vis spectrum with two bands located at c.a. 220 and 280 nm. The band at higher energy can be correlated to n→π* transition of C=O in the backbone of the protein (peptide bonds) and the band at lower energy comes from the amino acid side chains (phenyl rings in Trp, Tyr and Phe residues) and both are sensitive to conformational changes.[62]

UV/Vis absorption measurements are shown in Figure 8. In the system ligand-BSA (Figure 8, A), increasing concentrations of the ligand lead to an increase and a shift to lower wavenumber of the BSA band located at 280 nm. This change can be attributed to the contribution of the band belonging to the ligand (263 nm). Indeed, a comparison of the ligand spectrum (20 μM) mixed with BSA (6 μM) showed the presence of two bands located at 268 and 283 nm in which the band belonging to BSA slightly its intensity (Figure 8 A, inset). For the complex, the interaction seems to be different. The complex did not show the band at ~280 nm (Figure 8 C). The BSA band increased its intensity in contact with the complex and there was no significant change in the maximum at ~280 nm (Figure 8 B). These behaviors correlated with hydrophobic type of interaction that may possible happen, due to a π→π stacking between aromatic ring of the complex and the phenyl rings of aromatic aminoacids residues in the protein. In addition, the band at 220 nm slightly moved to higher wavelength suggesting changes in the polypeptide chain of BSA (Figure 8 B).

View Article Online
DOI: 10.1039/C9NJ01638D

Additional information can be obtained from the 3D fluorescence spectroscopy spectra. Peak 1 is the Rayleigh scattering peak (λex = λem). Peak A (λex = 280 nm, λem = 337.9 nm) is representative of Trp and Tyr residues, and the fluorescence intensity of the residues related with the polarity of the microenvironment (Figure 9A). Peak B (λex = 230 nm, λem=340.7 nm) is associated to the polypeptide backbone structure. As can be seen from Figures 9B and 9C, and Table 5, Peak A increased its intensity for the ligand and the complex, in comparison to BSA. Although quenching behavior is usually expected, sometimes the increment of fluorescence intensity occurs and is suggested to be due the increase of the quantum efficiency of the compound. This behavior has been previously observed and associated to an intercalative action of the ligands and complexes with NH groups.[63] It can be noted that the ligand 4-amino benzoic acid increased the intensity of Peak A more strongly than the complex.

The most remarkable change was observed for Peak B (Table 5). In the presence of the oxidovanadium(IV) complex this peak practically disappeared, in contrast to the ligand which intensity increased once more. The decrease of the band produced by the complex has been associated with changes in the peptide strands (unfolding). This causes the exposition of hydrophobic regions, together with a lowering of the α-helix content as a result of the impact of the interaction.[64] Thus, different kind of interactions were produced by the ligand and the complex, in agreement with the different observations in the UV/Vis spectra.

5. Conclusions

New oxidovanadium complexes containing vanadium(V) ($[VO(O_2)L(H_2O)]\cdot H_2O$) and (IV) ($[VOL_2H_2O]$) have been synthesized. The vanadium centers are both coordinated to 4-

View Article Online
DOI: 10.1039/C9NJ01638D

aminobenzoic in a bidentate mode through carboxylate group. The proposed structures were supported by computational data analysis based in DFT theory. For the oxidovanadium(IV) complex a *cis*-conformation was assumed in concordance with FTIR, UV/Vis and EPR spectroscopies. Related to the biological *in vitro* assays, the amino derivatives complexes behaved in a selective way with respect to the phosphatases inhibition: $[VOL_2H_2O]$ inhibited AcP, while $[VO(O_2)L(H_2O)]\cdot H_2O$ inhibited ALP. This inhibitory behavior was contrasted using FTIR spectroscopy demonstrating that in the presence of peroxidovanadium(V) complex ALP was not able to hydrolyze phosphate group belonging to the *p*-NPP and that action may be due to the strong loss of the α-helix conformation (~40%) in the Amide I band. In this work we focused the study in the chemistry of the complexes, their ability to inhibit ALP or AcP and followed the inhibition action by using FTIR spectroscopy. However, further studies are needed to elucidate the mechanism, type of inhibition and stability. Albumin interaction was investigated for the ligand and both complexes. Peroxidovanadium(V) complex produced a quenching effect on the fluorescence spectrum of BSA and their binding constant value denoted a static quenching process. Both the ligand and the oxidovanadium(IV) complex produced an enhancement of its fluorescence intensity after albumin interaction and the changes were evaluated through 3D fluorescence experiments which showed a more drastic rearrangement for the metal complex, because of the disappearance of Peak B, associated to the protein polypeptide backbone structure.

Conflicts of interest

There are no conflicts to declare.

Electronic Supplementary Information. Figure S1. Structure and selected bond lengths (Å) and angles (°) for *trans*-[VOL_2H_2O] complex. **Figure S2.** FTIR spectra of 4-aminobenzoic acid, sodium aminobenzoate, [VOL_2H_2O] and [$VO(O_2)L(H_2O)].H_2O$. **Figure S3**. Calculated bands in the UV-vis spectra of [$VO(O_2)L(H_2O)].H_2O$. **Figure S4.** Calculated bands in the UV-vis spectra of [VOL_2H_2O]. **Figure S5, S6 and S7.** Contour spectra and three-dimensional fluorescence spectra of 6 μM BSA**,** 6 μM BSA-20 μM 4-aminobenzoic acid and 6 μM BSA-20 μM [VOL_2H_2O], respectively.

Acknowledgments

This work was supported by Consejo Nacional de Investigaciones Científicas y Técnicas (CONICET, PIP 0611), Agencia Nacional de Promoción Científica y Tecnológica (ANPCyT, PICT16-1814), Universidad Nacional de La Plata (UNLP, X777) of Argentina. LGN and EGF are Research Fellows of CONICET. JEP and PAMW are Research Fellows of Comisión de Investigaciones Científicas de la Provincia de Buenos Aires (CICPBA) Argentina.

View Article Online
DOI: 10.1039/C9NJ01638D

Abbreviations

$[VO(O_2)L(H_2O)].H_2O$	$[VO(O_2)(C_7H_6NO_2)(H_2O)].H_2O$
$[VOL_2H_2O]$	$[VO(C_7H_6NO_2)_2H_2O]$
AcP	Acid phosphatase
ALP	Alkaline phosphatase
BSA	Bovine serum albumin
DMF	Dimethylformamide
DMSO	Dimethyl sulfoxide
p-NPP	Paranitrophenyl phosphate
Tris-HCl	Tris(hydroxymethyl)aminomethane hydrochloride

View Article Online
DOI: 10.1039/C9NJ01638D

Figures

Figure 1. Optimized geometry at the level of theory B3LYP/6-311+g* of oxidovanadium complexes: $[VO(O_2)L(H_2O)].H_2O$ (A, left) and *cis*-$[VOL_2H_2O]$ (B, right).

Figure 2. $[VO(O_2)L(H_2O)].H_2O$ complex: **(A) (a)** Diffuse reflectance spectrum in the 220-550 nm region, **(b)** peak fitting procedure with contribution of three involved bands; **(B) (a)** Electronic absorption spectra in the 260-600 nm region (2.7 x 10^{-3}M, DMF), **(b)** calculated spectrum, **(c)** peak fitting procedure with contribution of three involved bands.

Figure 3. [VOL_2H_2O] complex: **(A)** Diffuse reflectance spectrum in the 220-850 nm region, **(B)** Electronic absorption spectra in the 425-890 nm region (0.11 M, DMF), **(C)** Calculated *cis* and *trans* spectra.

Figure 4. (A) Powder EPR spectrum of $[VOL_2H_2O]$ obtained at 77 K, frequency 9.42 GHz; **(B)** Sample dissolved in DMF, at room temperature, in quartz flat cell, frequency 9.70 GHz.

Figure 5. Effect of 4-aminobenzoic acid (▼), $VOSO_4.5H_2O$ (■), $[VO(O_2)L(H_2O)].H_2O$ (▲), $[VO(O_2)]^+$ (♦) and $[VOL_2H_2O]$ (●) on **(A)** on AcP activity and **(B)** ALP activity. The values are expressed as the mean ± SEM of at least three independent experiments. *significant values in comparison with the basal level ($p < 0.05$)

Figure 6. FTIR changes in the finger print region (1230-840 cm^{-1}) of the substrate PNPP (4-nitrophenylphosphate): Liophilizated blank solution containing all the reactant except ALP enzyme (solid line); liophilizated blank solution containing all reactants including ALP enzyme (Dash line); all the reactant + $[VO(O_2)L(H_2O)].H_2O$ (■), all the reactant + $[VOL_2H_2O]$ (●) ; all the reactant + 4-aminobenzoic acid (L, ▲).

Figure 7. $[VO(O_2)L(H_2O)].H_2O$: left: Stern-Volmer plot F^0/F vs [Q], right: Plot of log $[(F^0-F)/F]$ vs log [Q].

Figure 8. UV-Vis spectra in the 220-300 nm region: (A) 4-aminobenzoic acid-BSA system (inset: deconvolution of the ~280 nm band), (B): $[VOL_2H_2O]$-BSA system (6 μM BSA, increasing concentrations of ligand and complex from 0-60μM), (C): solid line: 6 μM BSA, short dash: 6 μM BSA-20 μM aminobenzoic acid, gray line: 20 μM 4-aminobenzoic acid, dotted line: 6 μM BSA-20 μM $[VOL_2H_2O]$, dash dot line: 20 μM $[VOL_2H_2O]$.

Figure 9. Three-dimensional fluorescence spectra of 6 μM BSA, 6 μM BSA-20 μM 4-aminobenzoic acid and 6 μM BSA-20 μM $[VOL_2H_2O]$.

References

[1] K.H. Thompson and C. Orvig, *Dalton Trans.*, 2006, 761.

[2]. D.C. Crans and T.J. Meade, *Inorg. Chem.* 2013, **52**, 12181.

[3]. J. Costa Pessoa, S. Etcheverry and D. Gambino, *Coord. Chem. Rev.* 2015, **301–302,** 24.

[4]. D.C. Crans, L. Yang, A. Haase and X. Yang, *Met. Ions Life Sci.* 2018, **18**, 251.

[5] M. Sutradhar, L.M.D.R.S. Martins, M.F.C. Guedes da Silva and A.J.L. Pombeiro, *Coord Chem Rev*. 2015, **301-302**, 200.

[6] G. Süss-Fink, S. Stanislas, G.B. Shul'pin, G.V. Nizova, H. Stoeckli-Evans, A. Neels, C. Bobillier and S. Claude. *J. Chem. Soc*., *Dalton Trans*., 1999, 3169.

[7] G.R. Willsky, L-H Chia, M. Godzala III, P.J. Kostyniaka, J.J. Smeed, A.M. Trujillo, J.A. Alfano, W. Ding, Z. Huc and D.C. Crans. *Coord. Chem. Rev.* 2011, **255**, 2258.

[8] T. Koleša-Dobravc, K. Maejima, Y. Yoshikawa, A. Meden, H. Yasui and F. Perdih. *New J. Chem.,* 2018, **42**, 3619.

[9]. H. Cho, *Vitam. Horm.* 2013, **91**,405.

[10] M. al-Rashida1 and J. Iqbal, *Mini-Rev. Med. Chem.,* 2015**, 15***,* 41.

[11] N. Alimoradi, M.R. Ashrafi-Kooshk, M. Shahlaei, S. Maghsoudi, H. Adibi, R.P. McGeary and R. Khodarahmi, *J. Enz. Inhib. Med. Chem*. 2017, **32**, 20.

[12]. C. C. McLauchlan, B.J. Peters, G.R. Willsky and D.C. Crans, *Coord. Chem. Rev.* 2015, **301–302,** 163.

[13]. I.G. Fantus, S. Kadota, G. Deragon, B. Foster and B.I. Posner, *Biochemistry* 1989, **28**, 8864.

[14]. W. J. Geary. *Coord. Chem. Rev.* 1971, **7**, 81.

[15]. M. Samsonowicz, T. Hrynaszkiewicz, R. Świsłocka, E. Regulska and W. Lewandowski, *J. Mol. Struct.* 2005, **744–747**, 345.

[16]. U. Blum and G. Schwedt. *Anal. Chim. Acta* 1998, **360,** 101.

[17]. E.G. Ferrer, A. Bosch, O. Yantorno and E.J. Baran. *Bioorg. Med. Chem.* 2008, **16**, 3878.

[18]. M. Shahlaei, B. Rahimi, A. Nowroozi and M.R. Ashrafi-Kooshk. *Chem-Biol Interact.* 2015, **242,** 235.

[19]. M.J. Frisch, G.W. Trucks, H.B. Schlegel, G.E. Scuseria, M.A. Robb, J.R. Cheeseman, G. Scalmani, V. Barone, B. Mennucci, G.A. Petersson, H. Nakatsuji, M. Caricato, X. Li, H.P. Hratchian, A.F. Izmaylov, J. Bloino,G. Zheng, J.L. Sonnenberg, M. Hada, M. Ehara, K. Toyota, R. Fukuda, J. Hasegawa, M. Ishida, T. Nakajima, Y. Honda, O. Kitao, H. Nakai, T. Vreven, J.A. Montgomery Jr., J.E. Peralta, F. Ogliaro, M. Bearpark,

J.J. Heyd, E. Brothers, K.N. Kudin, V.N. Staroverov, T. Keith, R. Kobayashi, J. Normand, K. Raghavachari, A. Rendell, J.C. Burant, S.S. Iyengar, J. Tomasi, M. Cossi, N. Rega, J.M. Millam, M. Klene, J.E. Knox, J.B. Cross, V. Bakken, C. Adamo, J. Jaramillo, R. Gomperts, R.E. Stratmann, O. Yazyev, A.J. Austin, R. Cammi, C. Pomelli, J.W. Ochterski, R.L. Martin, K. Morokuma, V.G. Zakrzewski, G.A. Voth, P. Salvador, J.J. Dannenberg, S. Dapprich, A.D. Daniels, O. Farkas, J.B. Foresman, J.V. Ortiz, J. Cioslowski and D.J. Fox, Gaussian 09, Revision B.01, Gaussian, Inc, Wallingford CT, 2010.

[20]. Y. Zhao and D.G. Truhlar, *Theor. Chem. Acc.* 2007, **120**, 215.

[21]. M.E. Casida, Recent developments and applications in modern density functional theory, in: J.M. Seminario (Ed.), Theor. Comput. Chem, vol. 4, Elsevier, Amsterdam, 1996.

[22]. A.D. Becke, *Phys. Rev. A* 1988, **38,** 3098.

[23]. C. Lee, W. Yang and R.G. Parr, *Phys. Rev. B.* 1988, **37,** 785.

[24]. K. Nakamoto, Infrared and Raman Spectra of Inorganic and Coordination Compounds: Part A: Theory and Applications in Inorganic Chemistry, Sixth Edition, 2009, John Wiley and Sons.

[25]. J. Selbin. *Coord. Chem Rev.* 1996, **1**, 293.

[26]. S. Pacigová, R. Gyepes, J. Tatiersky and M. Sivák. *Dalton Trans.*, 2008, 121.

[27]. Infrared Spectral Interpretation. A systematic approach. B. Smith, 1999, CRC press LLC.

[28]. R. Swisłocka, M. Samsonowicz, E. Regulska and W. Lewandowski, *J. Mol. Struct.*, 2006, **792-793**, 227.

[29]. (a) A. E. Gerbase, M. Martinelli, L. G. Fagundes, V. Stefani and S. J. Da Silva, *J. Coord. Chem.*, 1999, **47**,451. (b) S. Pacigová, R. Gyepes, J. Tatiersky, M. Sivák. *Dalton Trans.* 2008, 121.

[30]. E. Lodyga-Chruscinska, D. Sanna, E. Garribba and G. Micera. *Dalton Trans.*, 2008, 4903.

[31]. J. Selbin, L. Morpurgo, *J. Inorg. Nucl. Chem.*, 1965, **27**, 673.

[32]. N.D. Chasteen (1981) In: Berliner LJ, Reuben J (eds) Biological magnetic resonance, vol 3. Plenum, New York.

[33]. G.R. Hanson, Y. Sun and C. Orvig. *Inorg. Chem.* 1996, **35**, 6507.

[34]. T. Jakusch, W. Jin, L. Yang, T. Kiss and D.C. Crans. *J. Inorg. Biochem.* 2003, **95**,1.

[35]. N. Mitic, S.J. Smith, A. Neves, L.W. Guddat, L.R. Gahan and G. Schenk. *Chem. Rev.* 2006, **106**, 3338.

[36]. C.C. McLauchlan, J.D. Hooker, M.A. Jones, Z. Dymon, E.A. Backhus, B.A. Greiner, N.A. Dorner, M.A. Youkhana and L.M. Manus. *J. Inorg. Biochem.* 2010, **104**, 274.

[37]. M. Li, W. Ding, B. Baruah, D.C. Crans and R. Wang, *J. Inorg. Biochem.* 2008, **102**, 1846.

[38]. J.J. Boruah, D. Kalita, S.P. Das, S. Paul and N.S. Islam, *Inorg. Chem.* 2011, **50**, 8046.

[39]. H. Sugiyama, S. Matsugo, H. Misu, T. Takamura, S. Kaneko, Y. Kanatani, M. Kaido, C. Mihara, N. Abeywardana, A. Sakai, K. Sato,Y. Miyashita and K. Kanamori, *J. Inorg. Biochem*. 2013, **121**, 66.

[40]. A. Ziegler, J. Florián, M.A. Ballicora and A.W. Herlinger, *J. Enzyme Inhibit Med. Chem*. 2009, 24,

[41]. C.M. Vescina, V.C. Sálice, A.M. Cortizo and S.B. Etcheverry, *Biol Trace Element Res.* 1996, 53, 185.

[42]. P. J. Stankiewicz and M.J. Gresser, *Biochemistry* 1988, **27**, 206.

[43]D.C. Crans, J.J. Smee, E. Gaidamauskas and L. Yang, *Chem. Rev.* 2004**, 104***,* 849.

[44] D. Crans, *J. Org. Chem*. 2015, **80**, 11899.

[45] A.P. Seale, L.A. de Jesus, S-Y Kim, Y-H Choi, H.B. Lim, C.-S Hwang and Y-S. Kim, *Biotechnol. Lett.* 2005, **27**, 221.

[46] L. Lu, X. Gao, M. Zhu, S. Wang, Q. Wu, S. Xing, X. Fu, Z. Liu and M. Guo, *Biometals* 2012, **25**, 599.

[47] J.D. Siqueira, A.C.O. Menegatti, H.Terenzi, M.B. Pereira, D. Roman, E.F. Rosso, P.C. Piquini, B.A. Iglesias and D.F. Back, *Polyhedron*, 2017, **130,** 184.

[48] J.J. Boruah, D. Kalita, S.P. Das, S. Paul and N.S. Islam, *Inorg. Chem*. 2011, **50,** 8046.

[49] A. Morinville, D. Maysinger and A. Shaver, *TiPS* 1998, **19**, 452.

[50] D.C. Crans, A.D. Keramidas, C. Drouza, *Phosphorus Sulfur Silicon Relat. Elem*.1996, **109**, 245.

[51]. B. Lendl, P. Krieg and R. Kellner, *Fresenius J. Anal. Chem.* 1998, **360**,717.

[52]. R. Vonach, B. Lendl and R. Kellner, *Analyst.,* 1997*,* **122,** 525.

[53]. P.T.T. Wong and D.W. Armstrong, *Biochim. Biophys. Acta,* 1992, **1159**, 237.

[54]. L. de La Fourniere, O. Nosjean, R. Buchet and B. Roux, *Biochim. Biophys. Acta*, 1995, **1248**, 186.

[55]. M. Bortolato, F. Besson and B. Roux, *PROTEINS: Structure, Function, and Genetics* 1999, **37**, 310.

[56]. S. Bem and W.S. Ostrowski, *Acta Biochim. Pol.* 2001, **48**, 755.

[57]. R. Gilmanshin, S. Williams, R.H. Callender, W.H. Woodruff and R. B. Dyer, *Proc. Natl. Acad. Sci. USA,*1997, 94, 3709.

[58]. K. Murayama and M. Tomida, *Biochem.* 2004, **43***,* 11526.

[59]. J.R. Lakowicz. Principles of fluorescence spectroscopy. New York: Plenum Press; 1983. p. 266e7.

[60]. U. Kragh-Hansen, V.T.G. Chuang and M. Otagiri, *Biol. Pharm. Bull.*2002, **25** 695.

[61]. P.D. Ross, S. Subramanian, *Biochem.* 1981, **20**, 3096.

[62]. Y. Wang, X. Wang, J. Wang, Y. Zhao, W. He and Z. Guo, *Inorg. Chem.* 2011, **50**, 12661.

[63]. Z. Mandegani, Z. Asadi, M. Asadi, H.R. Karbalaei-Heidari and B. Rastegari, *Dalton Trans.*, 2016, **45**, 6592.

[64]. Y. Wang, X. Wang, J. Wang, Y. Zhao, W. He and Z. Guo. *Inorg. Chem.* 2011, **50**, 12661.

View Article Online
DOI: 10.1039/C9NJ01638D

Table 1. Selected bond lengths (Å) and angles (º) around vanadium in the aminobenzoate (L) oxidovanadium complexes complex calculated at B3LYP 6-311+g*level of theory.

***cis*-[VOL_2H_2O]**[a]				**[$VO(O_2)L(H_2O)$].H_2O**			
Bond lengths (Å)		**angles (º)**		**Bond lengths (Å)**		**angles (º)**	
V-O1	1.597	O1VO2	110.2	V-O1	1.589	O1VO2	107.4
V-O2	2.016	O1VO3	108.5	V-O2	1.998	O1VO3	98.3
V-O3	2.017	O1VO4	103.2	V-O3	2.060	O1VO4	109.9
V-O4	2.021	O1VO5	158.9	V-O4	1.826	O1VO5	109.1
V-O5	2.269	O1VOw	93.8	V-O5	1.834	O1VOw	97.2
V-Ow	2.129	O2VO3	65.3	V-Ow	2.122	O2VO3	64.3
		O2VO4	144.9			O2VO4	133.4
		O2VO5	88.7			O2VO5	138.5
		O2VOw	93.4			O2VOw	76.4
		O3VO4	94.3			O3VO4	83.4
		O3VO5	87.5			O3VO5	127.4
		O3VOw	153.1			O3VOw	140.5
		O4VO5	60.9			O4VO5	45.6
		O4VOw	95.0			O4VOw	124.3
		O5VOw	75.2			O5VOw	80.2

[a]For the denomination of the atoms see Figure 1.

View Article Online
DOI: 10.1039/C9NJ01638D

Table 2. Characteristic FTIR bands for 4-aminobenzoic acid), its sodium salt, $[VO(O_2)L(H_2O)].H_2O$ and the calculated *cis*- and *trans*-$[VOL_2H_2O]$ isomers.(L=4-aminobenzoate ligand).

Aminobenzoic acid	**Benzoate sodium salt**	**$[VOL_2H_2O]$**			**$[VO(O_2)L(H_2O)].H_2O$**		**Assignments Main contributions**
Exp	**Exp**	**Exp**	**Calc. cis**	**Calc. trans**	**Exp**	**Calc.**	
1680(s)							**ν(C=O), (COOH)**
1626(s)	1633(s)	1693(w) 1634(sh)	1667.47 1659.57 1667.75 1659.67	1666.67 1657.46	1696(s)	1663.28 1655.26	**ν(CC), δ(NH_2)**
				1653.35	1603(m)	1637.82	**δH_2O**
1600(s)	1591(s)	1604(br.s)	1626.06 1615.11		1590(m)	1600.66	**ν(CC), δH_2O**
				1572.29			**ν(CC), δ(HCC)**
1522(s)	1529(vs)	1530(sh) 1506(m)	1525.37 1462.97		1525(m) 1498(w)	1574.35 1508.78	**$\nu_{as}(COO^-)$, ν(CC) δ(HCC)**
				1466.22 1454.07	1460(sh)	1479.87	**$\nu_{as}(COO^-)$,ν(CC), δ(HCC)**
	1397(s)	1408(s) 1390(sh)	1431.35 1396.85		1429(s)	1434.09	**$\nu_s(COO^-)$, ν(CC),**
1317(m)	1285(sh)	1315(w)	1359.07 1348.50	1359.77 1334.06	1378(m) 1315(sh) 1265(s)	1363.98 1326.21	**ν(NC) , δ(HCC)**
1171(s)	1173(s)	1181(m)	1208.34 1205.26	1206.39 1173.85	1185(sh) 1176(m)	1206.99 1170.38	**ν(CC),δ(HCC)**
1127(m)	1136(m)	1120(m) 1016(m)	1166.09	1155.48 1069.87	1127(m) 1112(m)	1151.31	**ν(CC),δ(HCC)**
1072(w)	1083(m)	1101(m)	1151.67 1073.24		1069(w)	1055.09	**δ(HCC), δ(HNC)**
		965(s)	1007.74	1014.48			**ν(V=O)**
					1017(m)	1021.06	**δ(CCC)**

					998(m)	979.96	**ν(V=O)+ν(O-O)**
					901(w)	884.92	**δ(CCC), δ(OCO) ν(CC),**
					871(m)	865.84	**τ(HCCC), τ(CCCC), γ(OCOC)**
		853(m)	868.90				**τ(HCCC), γ(OCOC)**
				868.68			**δ(CCC), γ(NCCC) δ(CCC)**
					844(m)	838.75	**δ(CCC), δ(OCO)**
		829(m)	838.93				**ν(CC), δ(OCO), δ(CCC)**
				835.56			**δ(OCO), δ(CCC)**
		769(m)	803.42				**δ(CCV),**
				803.19			**τ(HCCC), γ(OCOC)**
		668(w)	664.87	653.90			**δ(OCO)**
		638(w)	626.00				**δ(HOV)**
					691(m) 668(m) 658(w)	680.96 663.34 660.60	**τH_2O,δ(CCC), ν(VO_2)**
					630(m)	625.18	**δ(OOV), ν(VO_2)**
		542(w)	519.67				**τH_2O,τ(HCC)**
				518.50			**γ(NCCC)**
					560(m) 538(m)	566.08	**δ(CCO), δ(COV), τ(H_2O)**
		507(w)	502.18				**τ(HOVC)**
				509.36		478.62	**ν(V-C), τ(HOVC)**

1056 vs= very strong, s = strong, m = media, w = weak, vw = very weak, sh=shoulder, ν =
1057 stretching, δ = in-plane bending, γ = out-of-plane bending, τ=torsion.
1058

View Article Online
DOI: 10.1039/C9NJ01638D

Table 3. IC_{50} and K_m data values for a series of vanadium(IV) and (V) complexes containing NH group and/or comprising phenyl group structurally related to PNPP substrate.

Phosphatase	Compound	IC_{50}(μM)	K_m (μM)	
AcP[a] (sodium acetate, pH=4.8)	$VO(imc)_2$	-	3.3	[36]
	$VO_2(imc)_2^-$	-	33	[36]
	$VO(anc)_2$	-	23	[36]
	$VO_2(anc)_2^-$	-	0.25	[36]
AcP[b´] (acetate, pH=5.6)	$V(IV)O^{2+}$	67.37	-	This work
	$[VO(O_2)]^+$	63.45	-	This work
	$[VOL_2H_2O]$	250	-	This work
	$[VO(O_2)L(H_2O)]$	No inhibition		This work
ALP[c] (Tris, pH=7.8)				
	$VO(imc)_2$,	-	15.0	[36]
	$VO_2(imc)_2^-$	-	12.6	[36]
	$VO(anc)_2$	-	68	[36]
	$[VO(Big)_2].H_2O$,	33	-	[44]
	$[VO(Big1)_2].2H_2O$	17	-	[44]
	$V(IV)O^{2+}$	>500 μM	-	This work
	$[VO(O_2)]^+$	No inhibition	-	This work
	$[VOL_2H_2O]$	No inhibition	-	This work
	$[VO(O_2)L(H_2O)]$	500 μM	-	This work
ALP[d] (Glycine, pH=10)	$Na[VO(O_2)_2(H_2O)]$	25.18	9.13	[47]
	$[VO(O_2)_2$(sulfonate)]-PSS]	45.25	54.50	[47]
	$V_2O_2(O_2)_4$-(carboxylate)-$VO(O_2)_2$(sulfonate)]-PSSM	52.54	59.98	[47]
ALP[e] (HEPES, pH=8)	$NH_4[VO(O_2)$(dipic)$(H_2O)]]$	-	13.0	[49]
PTP1B (HEPES, pH=7.3)	$VO(imc)_2$	-	43	[36]
	$VO_2(imc)_2^-$	-	12.5	[36]
	$VO(anc)_2$	-	56.7	[36]
	$VO_2(anc)_2^-$	-	19.3	[36]
PTP1B (MOPS, pH=7)	$[VO(Big)_2].H_2O$,	8.6×10^{-4}	-	[45]
	$[VO(Big1)_2].2H_2O$	10.5×10^{-4}	-	[45]
	$VO(trop)_2$	0.76		[43]
	$VO(hino)_2$	0.27	0.15	[43]
PTP1B (imidazole, pH = 7.0)	$[VO_2(L^1)]_2[(Et)_3NH]_2$	1.51		[46]
	$[VO_2(L^2)]_2[(DBU\text{-}H)]_2$	lower inhibition		[46]

[a]Wheat Germen, [b´]Potato source, [c]Bovine calf intestine, MOPS pH = 7 for biguanido complexes and , [d]ALP = rabbit intestine, [e]ALP = chicken intestine, PTP1B = Protein-tyrosine phosphatase 1B. L = 4-aminobenzoate, imc = imidazole-4-carboxylate, anc = anthranilate (2-aminobenzoate); trp = tropolonato; hino = hinokitolonato, dipic = dipicolinic acid. HBig.HCl= N´,N´-dimethylbiguanide hydrochloride, Big1= phenformin, see scheme. PSS = poly(sodium 4-styrene sulfonate), PSSM = poly(sodium styrene sulfonate-*co*-maleate)]. L^1= 2,4-(dihydroxyphenyl)ethylidene)benzohydrazide, L^2 = bis[(3-hydroxy-5-(hydroxymethyl)-2-methylpyridin-4-l)methylene]oxalohydrazide; $(Et)_3NH$ = triethylamine; DBU = 1,8-diazabicyclo[5.4.0]undec-7-ene.

Table 4. FT-IR/ATR determination of secondary structure percentages of (i) ALP (glycine buffer pH=10.5) and (ii) AcP (acetate buffer) of the systems containing ALP with 4-aminobenzoic acid (ALP-L), $V(IV)O^{2+}$ (ALP-VO), oxidovanadium (ALP-[VOL_2H_2O]) and peroxidovanadium (ALP-[$VO(O_2)L(H_2O)].H_2O$) compound (500 μM).

Alkaline Phosphatase				
Amide I components	**% ALP-control**	**% ALP-L**	**% ALP-[VOL_2H_2O]**	**% ALP-[$VO(O_2)L(H_2O)].H_2O$**
β-antiparallel 1675-1695	3.41±0.03	9.74±0.07	8.21±0.06	8.94±0.07
Turns 1666-1673	10.99±0.13	6.20±0.05	8.82±0.07	7.57±0.03
α-helix 1650-1658	**39.59±0.45**	**34.25±0.41**	**33.08±0.38**	**24.22±0.30**
Random coil 1637-1645				
Solvated helix 1625-1637	24.9±0.29	29.87±0.31	30.17±0.36	36.77±0.22
β-sheet 1613-1625	21.10±0.17	19.97±0.18	24.09±0.20	22.37±0.27
Acid Phosphatase				
Amide I components	**%AcP-control**	**% AcP-L**	**%AcP-[VOL_2H_2O]**	**% AcP-[$VO(O_2)L(H_2O)].H_2O$**
β-antiparallel 1675-1695	7.60±0.20	13.05±0.27	14.87±0.23	12.94±0.25
Turns 1666-1673	16.95±0.31	9.98±0.17	15.10±0.32	12.02±0.19
α-helix 1650-1658	**34.37±0.80**	**29.96±0.90**	**20.77±0.57**	**32.06±0.64**
Random coil 1637-1645	26.8±0.38	25.01±0.56	**21.41±0.35**	26.57±0.42
Solvated helix 1625-1637	5.31±0.03	5.35±0.08	**21.85±0.27**	3.26±0.10
β-sheet 1613-1625	8.98±0.18	16.65±0.33	5.97±0.16	12.97±0.26

Averages (triplicates from separate samples) ±SE.

View Article Online
DOI: 10.1039/C9NJ01638D

Table 5: 3D Fluorescence Spectral Parameters of BSA, 4-amino benzoic acid-BSA and oxidovanadium(IV) complex-BSA system.

BSA

Peak position	λex/λem (nm/nm)	Δλ	Intensity
Peak A	280/337.9	57.9	4956.4
Peak B	230/340.7	110.7	575.8

4-amino benzoic acid-BSA system

Peak position	λex/λem (nm/nm)	Δλ	Intensity
Peak A	280/335.5	55.5	5721.2
Peak B	230/337.5	107.5	644.6

Oxidovanadium(IV)complex-BSA system

Peak position	λex/λem (nm/nm)	Δλ	Intensity
Peak A	280/337.2	57.2	5340.3
Peak B	230/-	-	-

Figure 1

View Article Online
DOI: 10.1039/C9NJ01638D

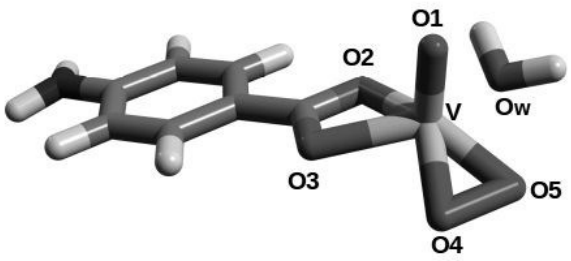

(A) $[VO(O_2)(C_7H_6NO_2)(H_2O)].H_2O$

($[VO(O_2)L(H_2O)].H_2O$)

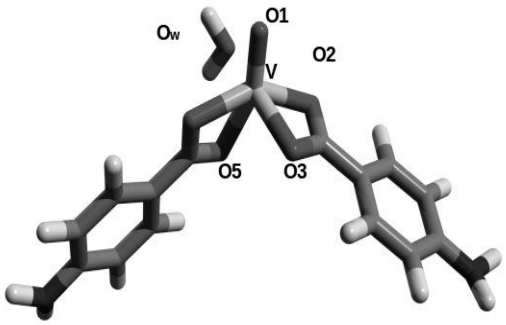

(B) *cis*-$VO(C_7H_6NO_2)_2H_2O$

(VOL_2H_2O)

Figure 2.

View Article Online
DOI: 10.1039/C9NJ01638D

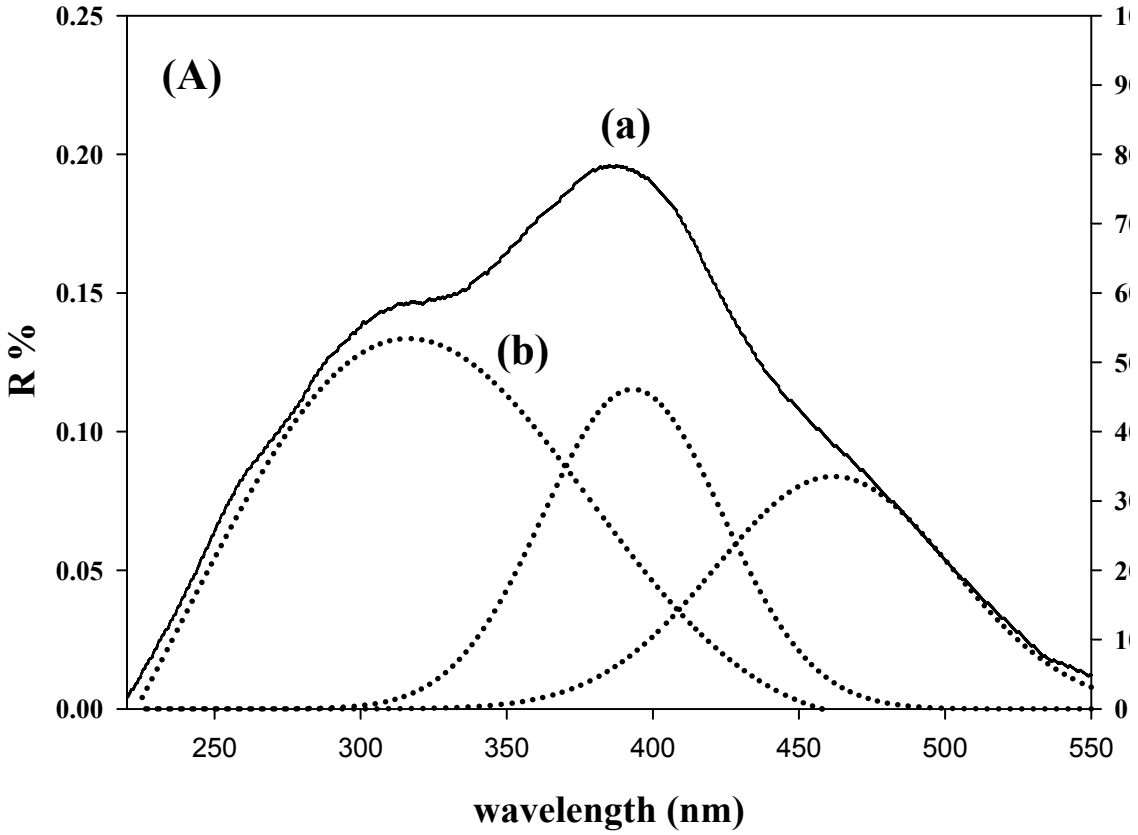

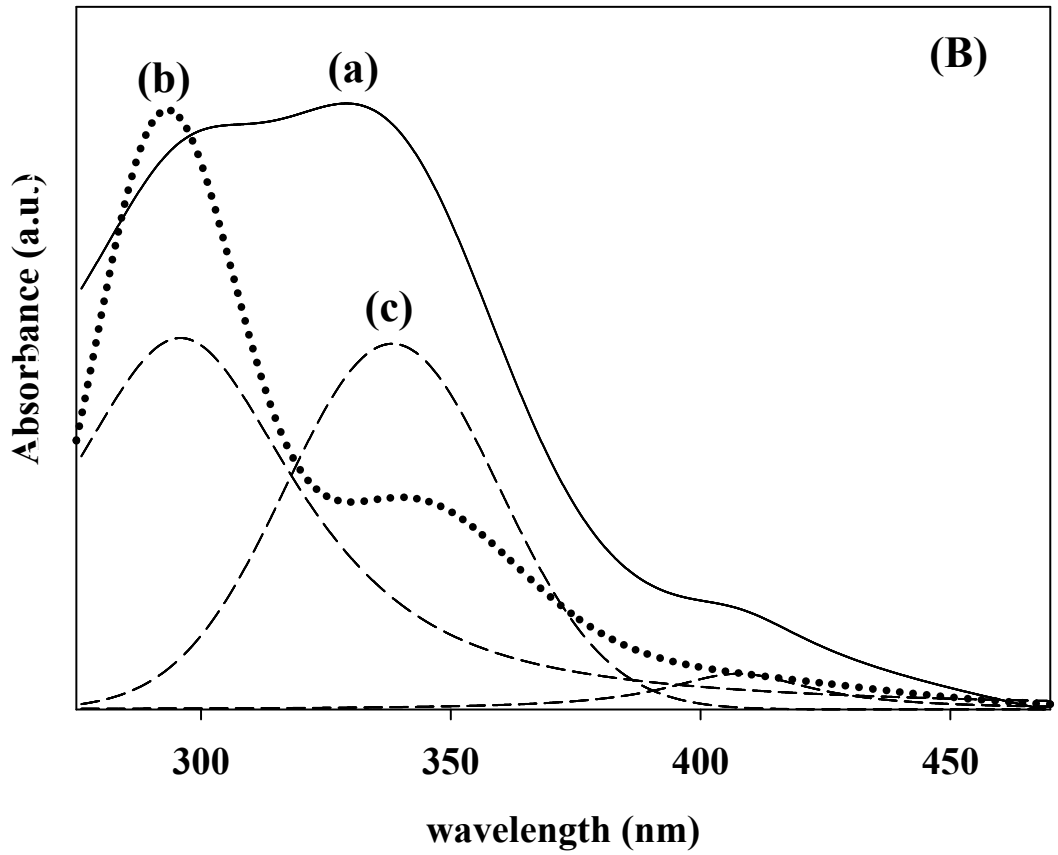

View Article Online
DOI: 10.1039/C9NJ01638D

Figure 3.

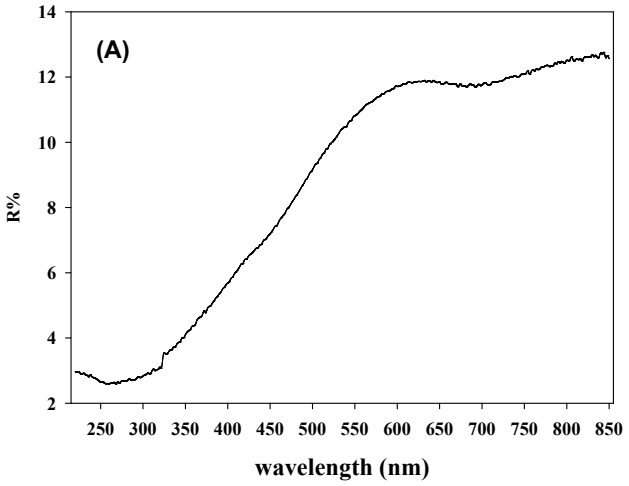

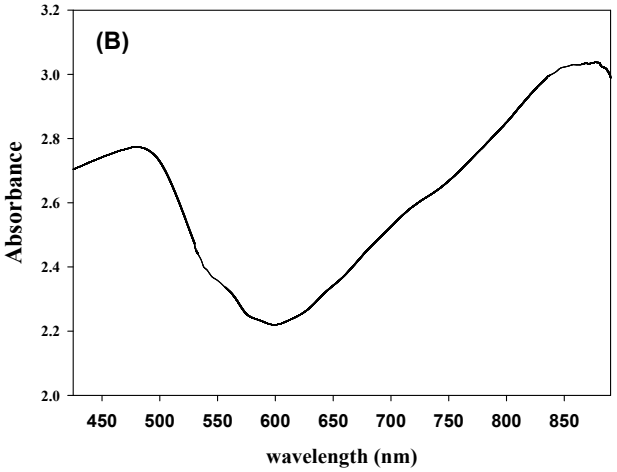

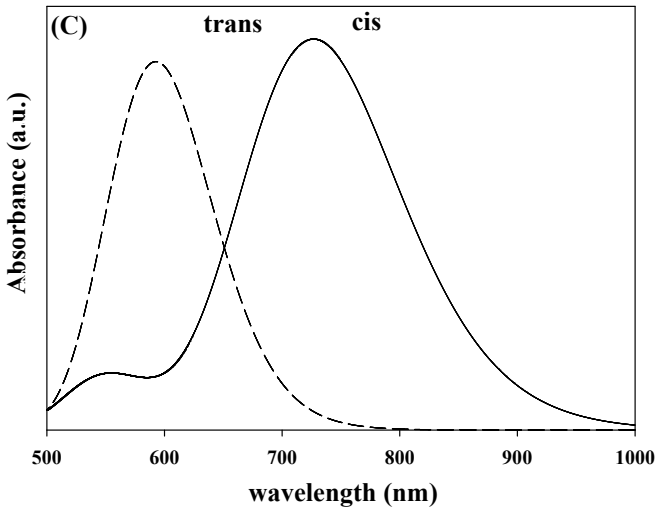

Figure 4

View Article Online
DOI: 10.1039/C9NJ01638D

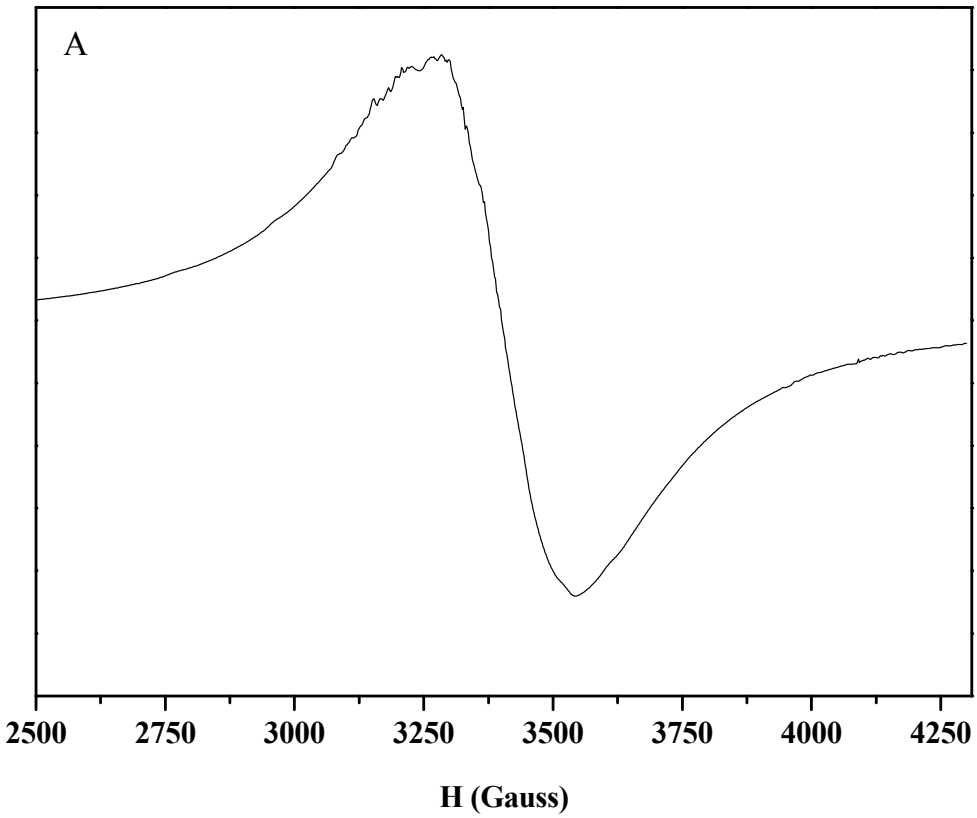

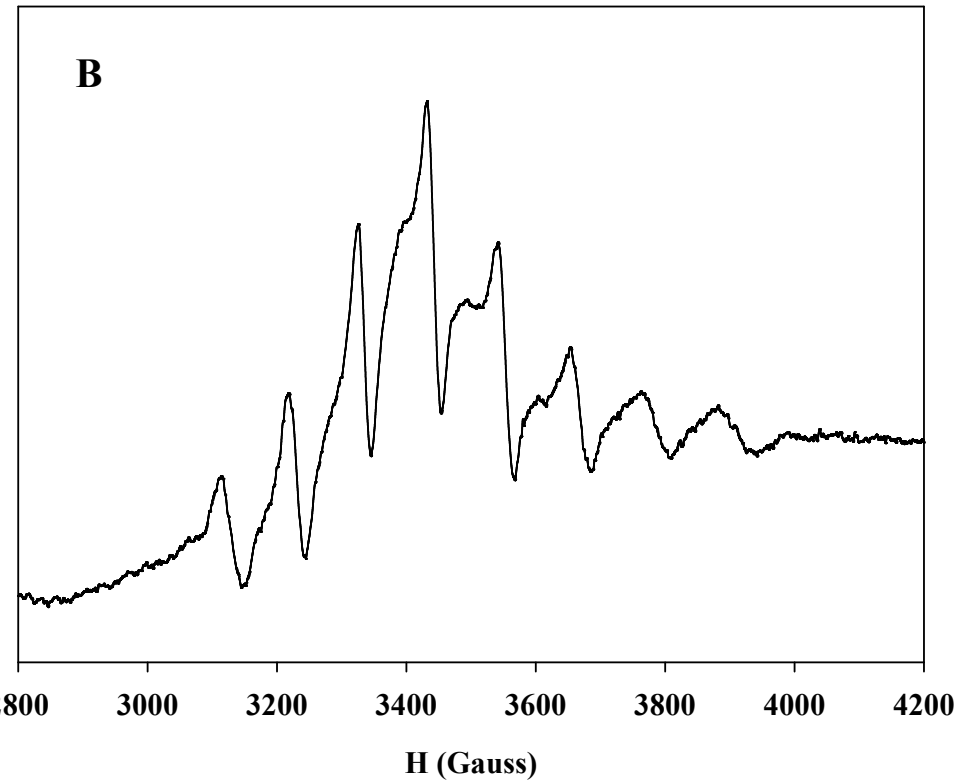

Figure 5

View Article Online
DOI: 10.1039/C9NJ01638D

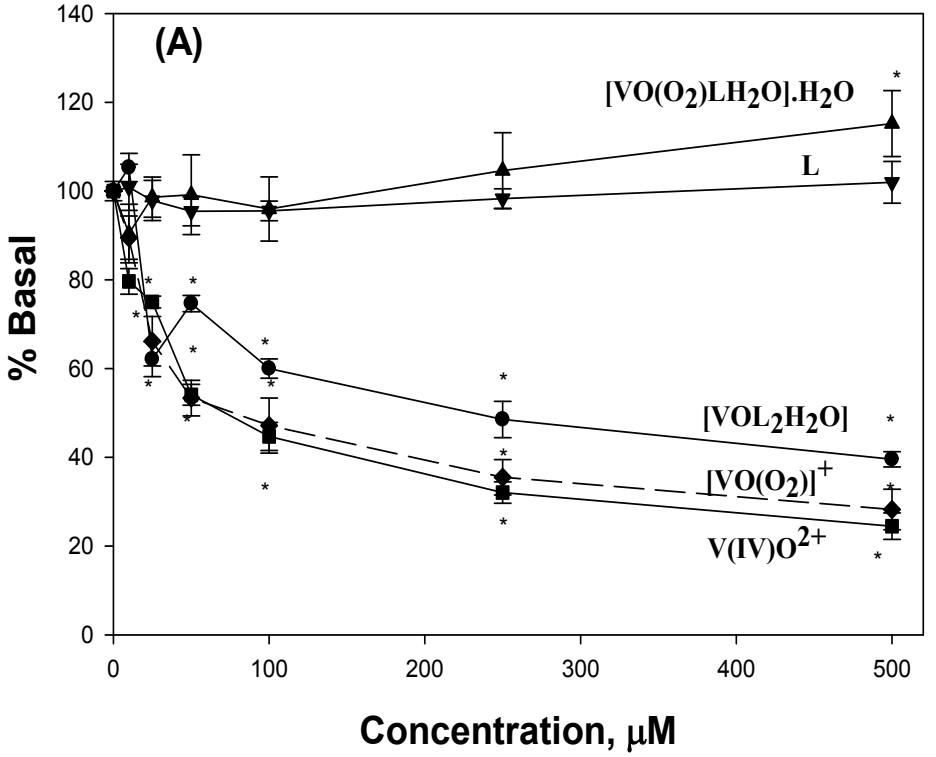

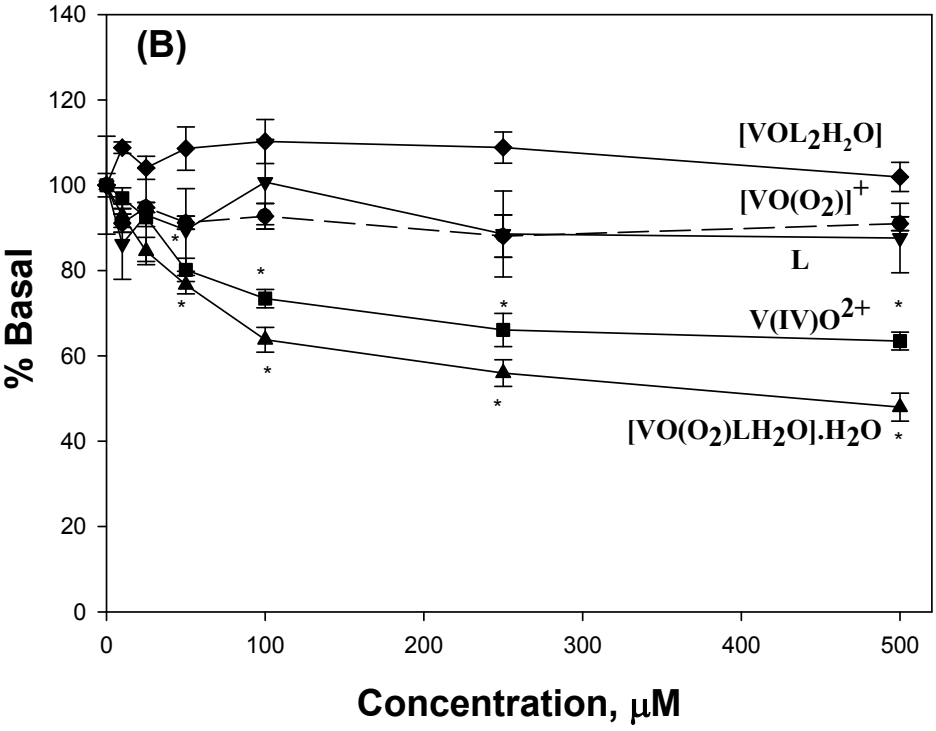

Figure 6.

View Article Online
DOI: 10.1039/C9NJ01638D

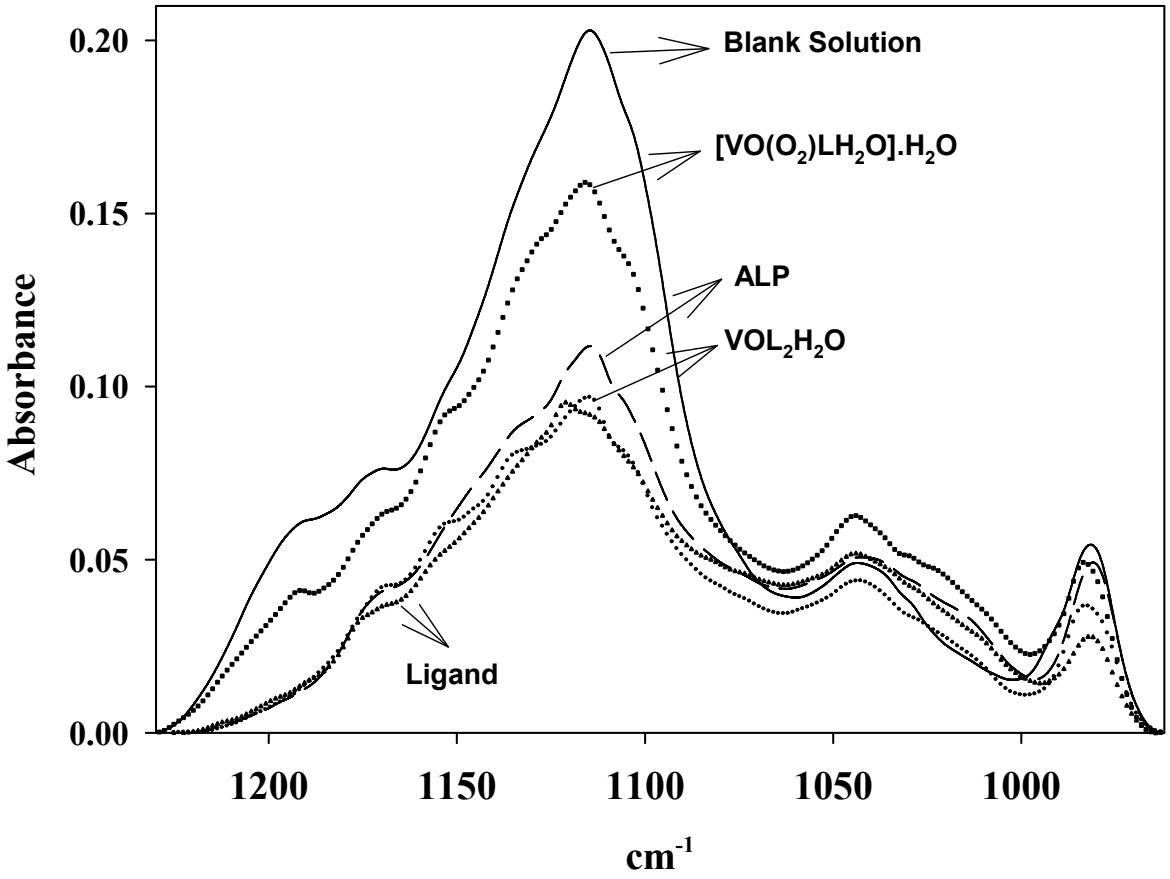

Figure 7

View Article Online
DOI: 10.1039/C9NJ01638D

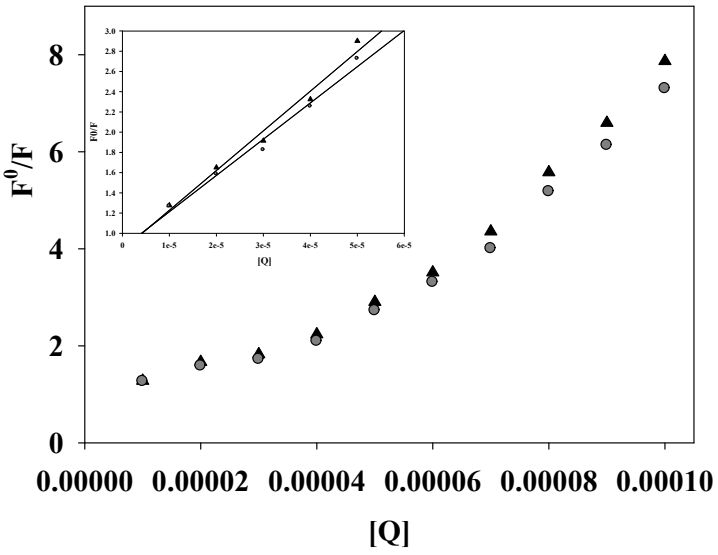

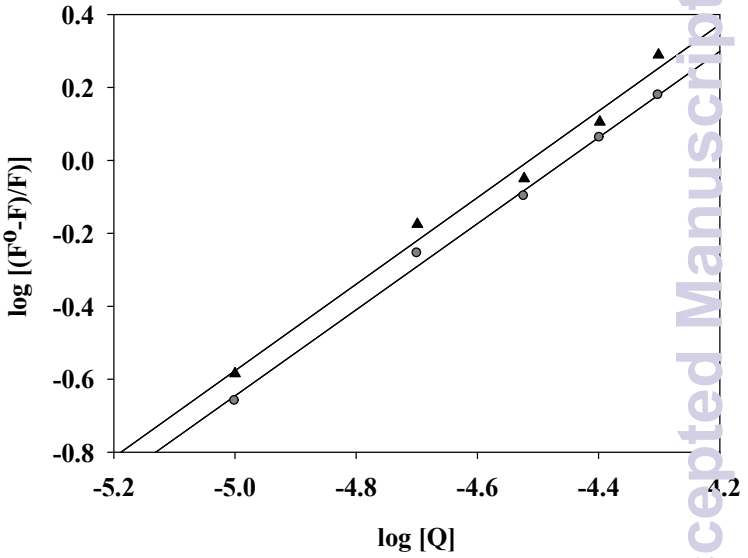

View Article Online
DOI: 10.1039/C9NJ01638D

Figure 8

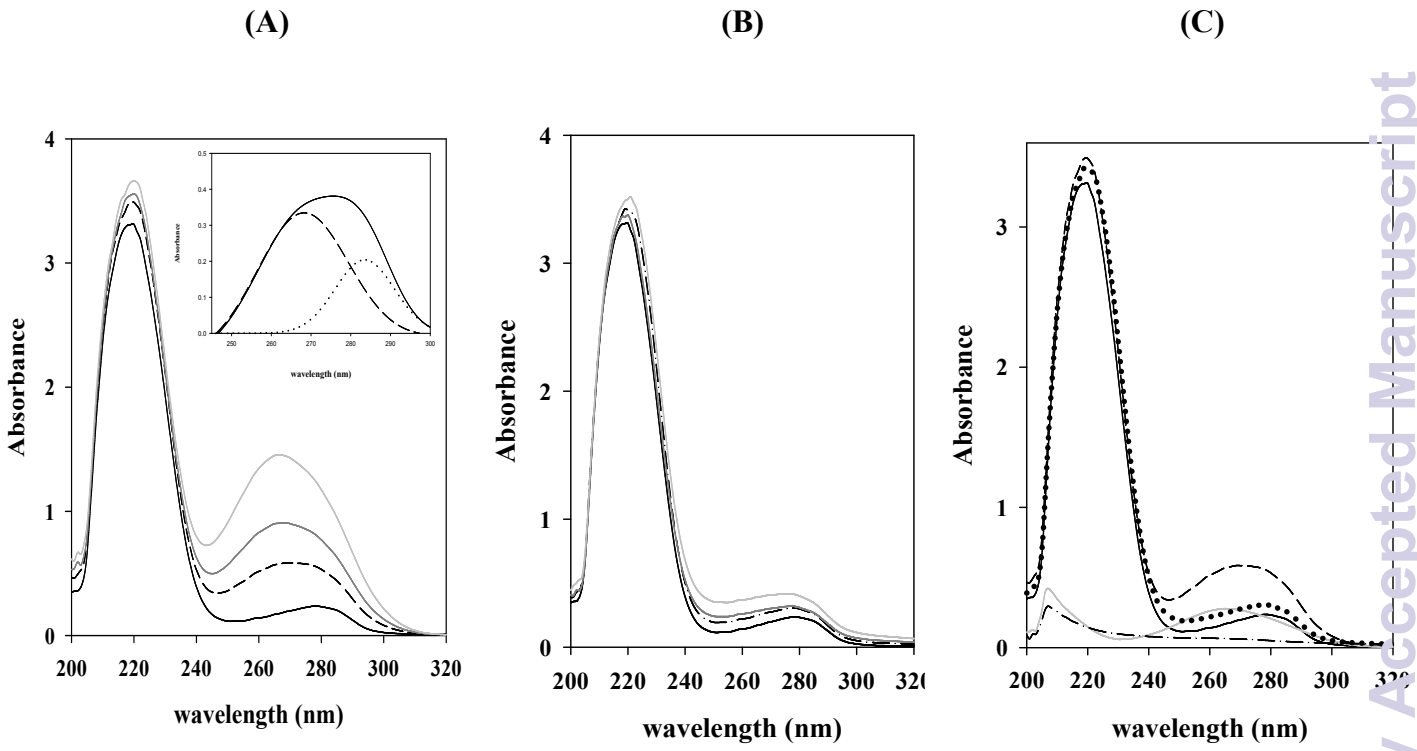

Figure 9